# Accepted Manuscript


New 6- and 7-heterocyclyl-1*H*-indole derivatives as potent tubulin assembly and cancer cell growth inhibitors

Giuseppe La Regina, Ruoli Bai, Antonio Coluccia, Valentina Naccarato, Valeria Famiglini, Marianna Nalli, Domiziana Masci, Annalisa Verrico, Paola Rovella, Carmela Mazzoccoli, Eleonora Da Pozzo, Chiara Cavallini, Claudia Martini, Stefania Vultaggio, Giulio Dondio, Mario Varasi, Ciro Mercurio, Ernest Hamel, Patrizia Lavia, Romano Silvestri

PII: S0223-5234(18)30376-3

DOI: 10.1016/j.ejmech.2018.04.042

Reference: EJMECH 10391

To appear in: *European Journal of Medicinal Chemistry*

Received Date: 20 February 2018

Revised Date: 19 April 2018

Accepted Date: 21 April 2018

Please cite this article as: G. La Regina, R. Bai, A. Coluccia, V. Naccarato, V. Famiglini, M. Nalli, D. Masci, A. Verrico, P. Rovella, C. Mazzoccoli, E. Da Pozzo, C. Cavallini, C. Martini, S. Vultaggio, G. Dondio, M. Varasi, C. Mercurio, E. Hamel, P. Lavia, R. Silvestri, New 6- and 7-heterocyclyl-1*H*-indole derivatives as potent tubulin assembly and cancer cell growth inhibitors, *European Journal of Medicinal Chemistry* (2018), doi: 10.1016/j.ejmech.2018.04.042.

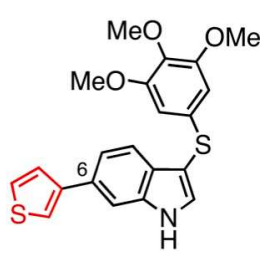


| | $IC_{50}$ |
|---|---|
| Tubulin | 0.58 μM |
| MCF-7 | 4.5 nM |
| HT-29 | 10 nM |
| PC3 ($GI_{50}$) | 3.5 nM |
| ADR/RES | 7.5 nM |

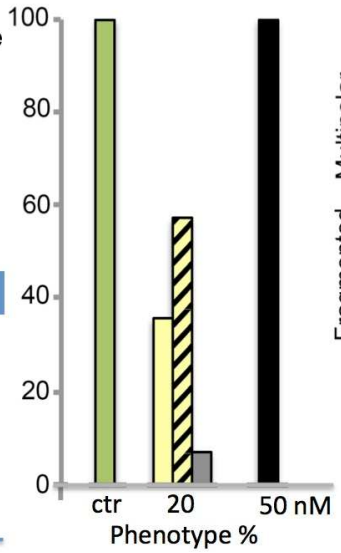


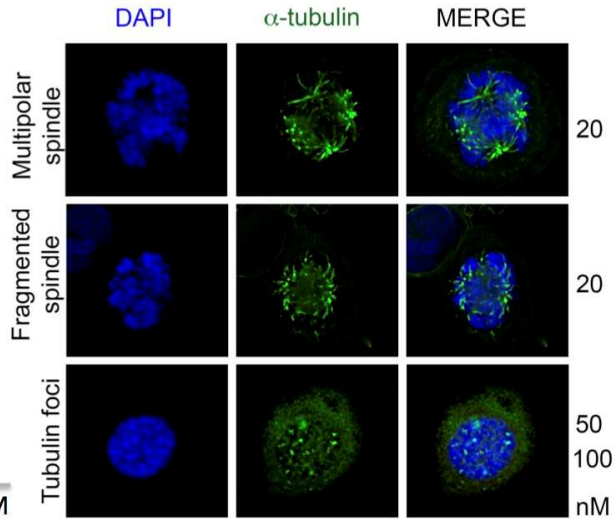

# New 6- and 7-heterocyclyl-1*H*-indole derivatives as potent tubulin assembly and cancer cell growth inhibitors

Giuseppe La Regina,[a] Ruoli Bai,[b] Antonio Coluccia,[a] Valentina Naccarato,[a] Valeria Famiglini,[a] Marianna Nalli,[a] Domiziana Masci,[a] Annalisa Verrico,[c] Paola Rovella,[c] Carmela Mazzoccoli,[d] Eleonora Da Pozzo,[e] Chiara Cavallini,[e] Claudia Martini,[e] Stefania Vultaggio,[f] Giulio Dondio,[g] Mario Varasi,[f] Ciro Mercurio,[f] Ernest Hamel,[b] Patrizia Lavia,[c] and Romano Silvestri[a,*]

[a] *Department of Drug Chemistry and Technologies, Sapienza University of Rome, Laboratory affiliated to Istituto Pasteur Italia – Fondazione Cenci Bolognetti, Piazzale Aldo Moro 5, I-00185 Roma, Italy*

[b] *Screening Technologies Branch, Developmental Therapeutics Program, Division of Cancer Treatment and Diagnosis, Frederick National Laboratory for Cancer Research, National Cancer Institute, National Institutes of Health, Frederick, Maryland 21702, United States*

[c] *Institute of Molecular Biology and Pathology (IBPM), CNR Consiglio Nazionale delle Ricerche, c/o Sapienza University of Rome, Via degli Apuli 4, I-00185 Roma, Italy*

[d] *Laboratorio di Ricerca Pre-Clinica e Traslazionale, Istituto di Ricovero e Cura a Carattere Scientifico (IRCCS), Centro di Riferimento Oncologico della Basilicata, Via Padre Pio 1, I-85028 Rionero in Vulture, Italy*

[e] *Department of Pharmacy, University of Pisa, Via Bonanno Pisano 6, I-56126 Pisa, Italy*

[f] *Experimental Therapeutics IFOM-the FIRC Institute of Molecular Oncology Foundation, Via Adamello 16, 20139 Milan, Italy*

[g] *APHAD, Via della Resistenza 65, 20090 Buccinasco (MI), Italy*

* Corresponding author

*e-mail address:* romano.silvestri@uniroma1.it; *phone:* +39 06 4991 3800

*Keywords:*
Microtubule
Tubulin
Cancer cell
Inhibitor
Indole

## ABSTRACT

We designed new 3-arylthio- and 3-aroyl-1*H*-indole derivatives **3-22** bearing a heterocyclic ring at position 5, 6 or 7 of the indole nucleus. The 6- and 7-heterocyclyl-1*H*-indoles showed potent inhibition of tubulin polymerization, binding of colchicine to tubulin and growth of MCF-7 cancer cells. Compounds **13** and **19** inhibited a panel of cancer cells and the NCI/ADR-RES multidrug resistant cell line at low nanomolar concentrations. Compound **13** at 50 nM induced 77% G2/M in HeLa cells, and at 20 nM caused 50% stable arrest of mitosis. As an inhibitor of HepG2 cells ($IC_{50}$ = 20 nM), **13** was 4-fold superior to **19**. Compound **13** was a potent inhibitor of the human U87MG glioblastoma cells at nanomolar concentrations, being nearly one order of magnitude superior to previously reported arylthioindoles. The present results highlight **13** as a robust scaffold for the design of new anticancer agents.

## 1. Introduction

Microtubules (MTs) are hollow, cylindrical, filamentous structures made of dimerized α- and β-tubulin subunits and are characterized by a highly dynamic equilibrium involving polymerization, where tubulin dimers bind non-covalently to a MT, and depolymerization to tubulin dimers [1]. MTs regulate key cellular functions, such as cell growth and division, intracellular trafficking, preservation of the architecture of the cell, and motility. Due to these key roles, disrupting the dynamic equilibrium of MTs at either the tubulin assembly or MT disassembly level, results in a fatal cellular event. Cancer cells are characterized by a high rate of cell division: hence, the strategy of inducing cell death through an interference with the dynamics of MTs has proved successful for the design of effective antitumor drugs [2-6].

MT binding agents fall into two main groups: (i) inhibitors of tubulin polymerization, including colchicine [7,8], combretastatin A-4 (CSA4) [9] (Chart 1), vincristine (VCR), vinorelbine (VRB) and vinblastine (VBL); and (ii) MT stabilizers, including taxoids and epothilones. The stabilizers stimulate MT polymerization and stabilization at high concentrations, whereas at lower concentrations paclitaxel (PTX) inhibits MT dynamics with little effect on the proportion of tubulin in polymer [10]. Taxoids and epothilones bind at a luminal site on the β-subunit [11,12] following entry into the MT through pores in its wall [13] that are shaped by various tubulin subunits on the MT surface. Some evidence indicates a transient binding of MT stabilizers at a specific pore site.

Despite considerable clinical successes [14,15], the anticancer therapies based on tubulin binding agents still have limitations perhaps due to multi-drug resistance (MDR), toxicity and unwanted side effects [16,17]. Therefore, there is a quest for new effective MT inhibitors with fewer side effects to become components of improved anticancer treatments [18,19].

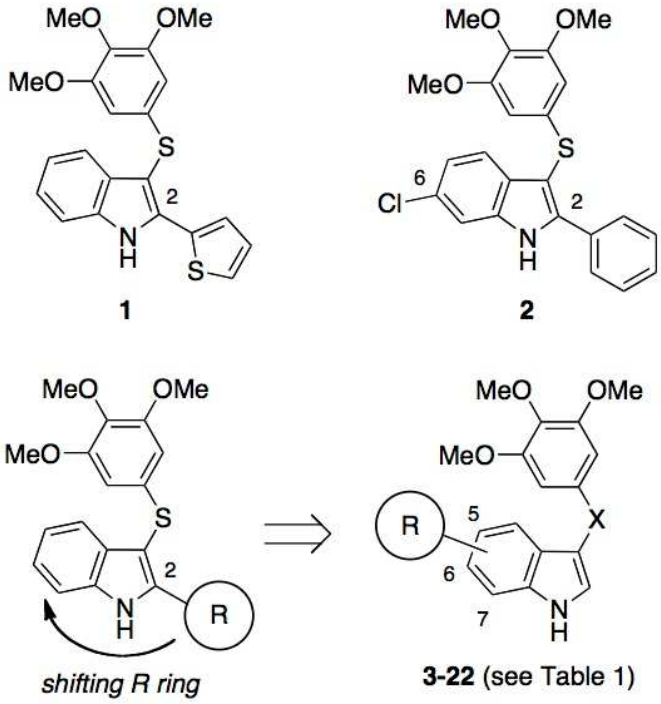


**Chart 1.** Structures of compounds **1−22.**

Currently, there are no US Food and Drug Administration approved anticancer drugs on the market binding at the colchicine site [20]. Compared to other tubulin agents, these compounds (i) have shown less transporter mediated drug resistance in preclinical studies [21], (ii) are minimally affected by the overexpression of βIII-tubulin [22], and (iii) have generally better water solubility [9].

Improvements of activity of colchicine site binding agents by replacement or introduction of heterocyclic ring(s) to the parent scaffold have been reported [16,23,24]. Accordingly, as tubulin polymerization inhibitors, 2-heterocyclyl-3-arylthio-1*H*-indole (2-HATI) derivatives were more effective than the corresponding 2-aryl-3-arylthio-1*H*-indole counterparts in both the sulfur and

aroyl series [25]. For example, 2-(thiophen-2-yl)-3-[(3′,4′,5′-trimethoxyphenyl)thio]-1*H*-indole (**1**) inhibited tubulin assembly with an $IC_{50}$ of 0.74 μM and MCF-7 cancer cell growth with an $IC_{50}$ of 39 nM [26]. Compound **1** was superior to VRB, VBL, and PTX as an inhibitor of the P-glycoprotein (Pgp) overexpressing NCI/adriamycin-resistant (ADR-RES) MDR cell line and showed satisfactory metabolic stability. Recently, introduction of halogen or methoxy substituent(s) at positions 4−7 of 3-arylthio-1*H*-indoles (ATIs) bearing the phenyl at position 2 of the indole provided potent tubulin polymerization inhibitors (for example **2**) [27].

Herein we report the synthesis of new indole derivatives **3-22** bearing a five-membered heterocyclic ring at position 5, 6 or 7 of the indole ring (Chart 1 and Table 1). Our findings demonstrate that the new derivatives are potent anticancer agents, superior to the corresponding reference derivative **1** [26]. Compounds **13** and **19** inhibited the HT29, HCT116, HepG2, T98G, U87MG, U343G and NCI/ADR-RES cell lines with $IC_{50}$ values in the nanomolar range. Compound **13** was superior to the previously reported compounds [26] as an inhibitor of HepG2 and glioblastoma cells.

## 2. Chemistry

### *2.1. Synthetic procedures*

Arylthioindoles **3-7**, **9**, **11**, **13**, **15**, **19** and **37** were prepared according to our previously reported venting-while-heating microwave (MW)-assisted procedure [28] by treating the appropriate indole with bis(3,4,5-trimethoxyphenyl)disulfide [29] in the presence of sodium hydride in anhydrous *N*,*N*-dimethylformamide (DMF) at 130 °C for 2 min (120 W) (Scheme 1). Reaction of the indole with 3,4,5-trimethoxybenzoyl chloride in the presence of diethylaluminum chloride in dichloromethane at -10 °C for 2 h furnished methanones **8**, **10**, **12** and **14**. Derivatives **16-18**, **20-22**, **30-32**, **35** and **36** were synthesized by a coupling reaction of the appropriate indole

with the boronic derivative in the presence of tris(dibenzylideneacetone)dipalladium(0) ($Pd_2dba_3$), 2-dicyclohexylphosphino-2′,6′-dimethoxybiphenyl (SPhos) and potassium phosphate tribasic in 1-butanol at 100 °C for 15 h. A palladium(II) acetate ($Pd(OAc)_2$)-catalyzed reaction of 5-iodo-1*H*-indole (**24**) with 2-furanboronic or 2-thienylboronic acid in the presence of tri(*o*-tolyl)phosphine ($P(o\text{-tol})_3$) and potassium phosphate tribasic in ethanol/toluene at 80 °C for 2 h gave the corresponding heteroaryl indoles **27** and **29**, respectively. MW-assisted treatment of indole **24** with 3-furanboronic acid pinacol ester in the presence of $Pd(OAc)_2$ and potassium carbonate in methylpyrrolidone/water at 110 °C for 15 min (200 W) furnished 5-(furan-2-yl)-1*H*-indole (**28**). Compound **38** was prepared by MW-assisted Friedel-Crafts reaction of 7-iodo-1*H*-indole (**26**) with 3,4,5-trimethoxybenzoyl chloride in the presence of anhydrous aluminum chloride in 1,2-dichloroethane at 110 °C for 2 min (150 W).

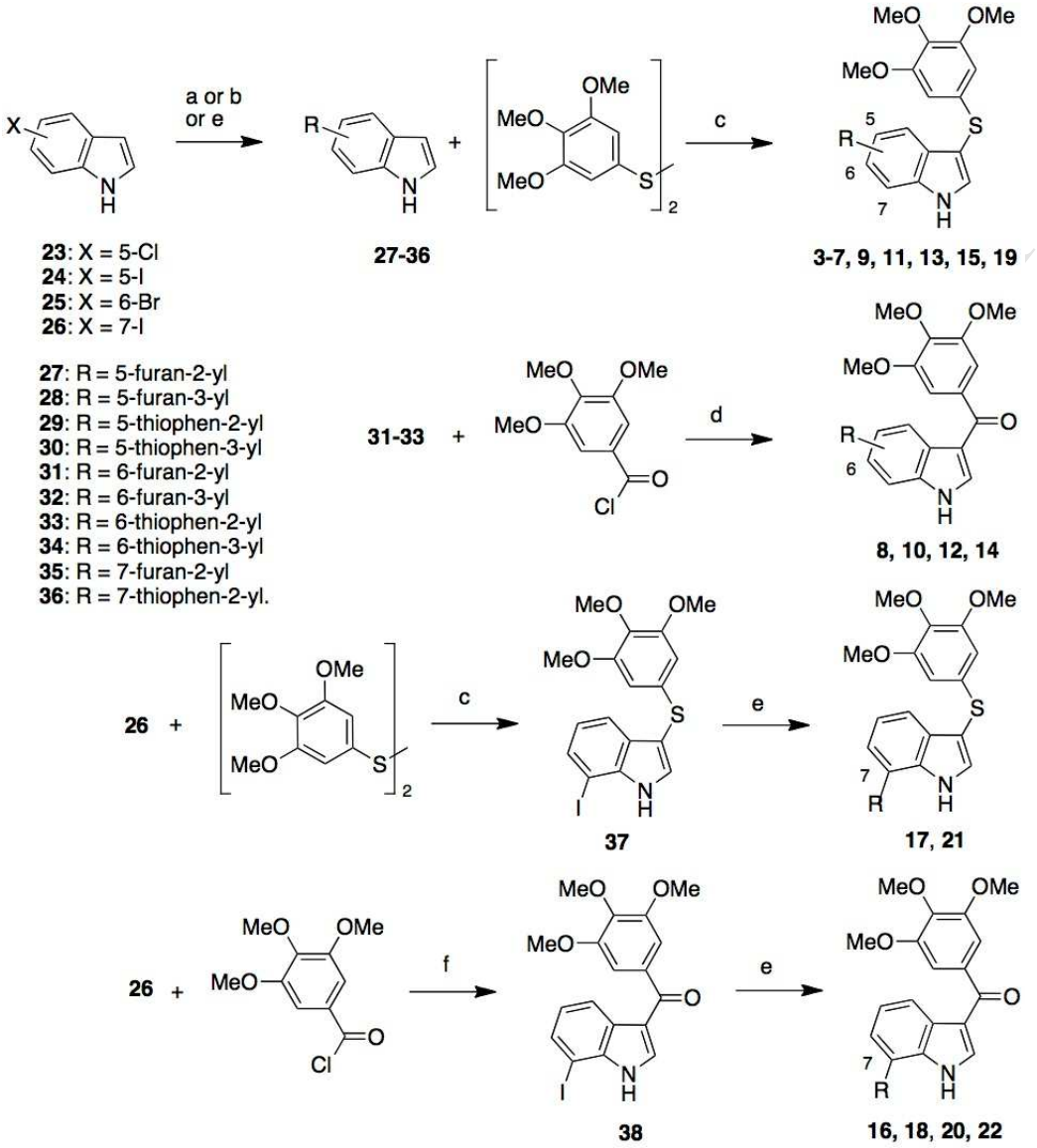


**Scheme 1.** Synthesis of Compounds **3-22** and **27-37**. Reagents and reaction conditions: (a) (**27**, **29**) boronic derivate, $Pd(OAc)_2$, P(*o*-tol)$_3$, $K_3PO_4$, EtOH/PhMe, 80 °C, 2 h, 73-87%; (b) (**28**) 3-furanboronic acid pinacol ester, $Pd(OAc)_2$, $K_2CO_3$, methylpyrrolidone/water, closed vessel, 200 W, 110 °C, 15 min, 45%; (c) (**3-7, 9, 11, 13, 15, 19** and **37**) bis(3,4,5-trimethoxyphenyl)disulfide, NaH, anhydrous DMF, closed vessel, 120 W, 130 °C, 2 min, 5-50%; (d) (**8, 10, 12, 14**) (*i*) diethylaluminum chloride, $CH_2Cl_2$, -78 °C, Ar stream; (*ii*) 3,4,5-trimethoxybenzoyl chloride, -10 °C → 25 °C within 2 h, 14-69%; (e) (**16-18, 20-22, 30-32**, **35** and **36**) boronic derivative, $Pd_2dba_3$, SPhos, $K_3PO_4$, BuOH, 100 °C, 15 h, 5-75%; (f) (**38**) 3,4,5-trimethoxybenzoyl chloride, $CH_2Cl_2$, anhydrous $AlCl_3$, closed vessel, 150 W, 110 °C, 2 min, 51%.

**Table 1**
Inhibition of tubulin polymerization, growth of MCF-7 human breast carcinoma cells, and colchicine binding by compounds **3-22**.[a]

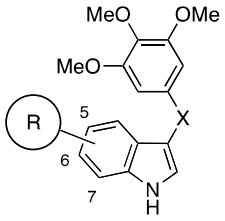


**3-22**

| Compd | R | X | $IC_{50}$ ± SD (μM) | $IC_{50}$ ± SD (nM) | (% ± SD) |
|---|---|---|---|---|---|
| | | | Tubulin[b] | MCF-7[c] | Inh. Colch. Bind.[d] |
| **3** | 5-  | S | 0.87 ± 0.1 | 70 ± 10 | 81 ± 1 |
| **4** | 5-  | S | 1.8 ± 0.1 | 200 ± 100 | 63 ± 1 |
| **5** | 5-  | S | 1.3 ± 0.09 | 150 ± 70 | 76 ± 2 |
| **6** | 5-  | S | 1.7 ± 0.03 | 200 ± 0 | 72 ± 3 |
| **7** | 6-  | S | 0.59 ± 1 | 10 ± 3 | 97 ± 1 |
| **8** | 6-  | C=O | 0.76 ± 0.04 | 4.7 ± 0.6 | 96 ± 0.1 |
| **9** | 6-  | S | 2.3 ± 0.04 | 10 ± 0 | 90 ± 2 |
| **10** | 6-  | C=O | 0.61 ± 0.06 | 4.3 ± 0.6 | 96 ± 0.1 |
| **11** | 6-  | S | 0.47 ± 0.05 | 6.0 ± 1 | 95 ± 1 |
| **12** | 6-  | C=O | 0.38 ± 0.1 | 9.6 ± 0.6 | 96 ± 0.8 |
| **13** | 6-  | S | 0.58 ± 0.06 | 4.5 ± 1 | 97 ± 0.3 |
| **14** | 6-  | C=O | 0.60 ± 0.04 | 18 ± 4 | 94 ± 0.6 |
| **15** | 7-  | S | 0.64 ± 0.06 | 15 ± 4 | 95 ± 0.6 |

| | | | | | |
|---|---|---|---|---|---|
| **16** | 7-  | C=O | 1.9 ± 0.03 | 320 ± 10 | 70 ± 1 |
| **17** | 7-  | S | 1.3 ± 0.1 | 24 ± 2 | 86 ± 1 |
| **18** | 7-  | C=O | 3.0 ± 0.3 | 1300 ± 0 | 29 ± 0.6 |
| **19** | 7-  | S | 0.57 ± 0.03 | 29 ± 1 | 89 ± 1 |
| **20** | 7-  | C=O | 2.6 ± 0.04 | 550 ± 70 | 48 ± 0.5 |
| **21** | 7-  | S | 1.3 ± 0.01 | 38 ± 10 | 77 ± 0.1 |
| **22** | 7-  | C=O | 6.2 ± 1 | 1400 ± 100 | Nd[e] |
| **1** | — | — | 0.74 ± 0.05 | 39 ± 10 | 88 ± 2 |
| Colch. | — | — | 3.2 ± 0.4 | 5 ± 1 | — |
| CSA4 | — | — | 1.0 ± 0.1 | 13 ± 3 | 98 ± 0.6 |

[a] Experiments were performed in duplicate or triplicate.
[b] Inhibition of tubulin polymerization. Tubulin was at 10 μM in the assembly assay.
[c] Inhibition of growth of MCF-7 human breast carcinoma cells.
[d] Inhibition of [$^3$H]colchicine binding: tubulin, [$^3$H]colchicine, inhibitor at 1:5:5 μM.
[e] Nd, not done.
[f] CSA4 yielded $IC_{50}$ of 0.65 ± 0.03 μM in the assay with **5-7**, **10**, **12**, **15** and **17**, and $IC_{50}$ of 0.64 ± 0.01 μM in the assay with **9** and **11**, in which different tubulin preparations were used.

## 3. Results and discussion

### *3.1. Inhibition of tubulin polymerization*

We synthesized arylthioindole and aroylindole derivatives **3-22** to explore the effects of five-membered heterocyclic rings at position 5, 6 or 7 of the indole nucleus (Table 1). Ten new derivatives (**3**, **7**, **8**, **10-15**, and **19**) inhibited tubulin polymerization with $IC_{50}$ values at submicromolar concentrations, six compounds (**4-6**, **16**, **17** and **21**) were in the 1.0−2.0 μM range, as compared with colchicine ($IC_{50}$ = 3.2 μM) and CSA4 ($IC_{50}$ = 1.0 μM). With the

exception of **9**, the most potent tubulin polymerization inhibitors (**7**, **8** and **10-14**) were characterized by the presence of the heterocyclic ring at position 6 of the indole; among others, compound **3**, with the heterocyclic ring at position 5 of the indole, and **16**, **17** and **21**, with the heterocyclic ring at position 7, showed $IC_{50}$ values <1.0 μM. As tubulin assembly inhibitors, the compounds bearing the furanyl-2-yl or the thiophen-2-yl ring were generally superior to the corresponding furan-3yl-/thiophen-3-yl derivatives (compare **3** with **4**, **5** with **6**, **7** with **9**, **15** with **17**, and **19** with **21**). Replacement of the sulfur bridging atom with the carbonyl group also provided potent tubulin assembly inhibitors. The presence of the heterocycle at position 7 of the indole conferred significant differences of inhibition of tubulin polymerization among arylylthio/aroyl derivatives (compare **15** with **16**, **17** with **18**, **19** with **20**, and **21** with **22**), while compounds **7-14** with the heterocycle at position 6 were almost equipotent, except **9** and **10**, with **12** ($IC_{50}$ = 0.38 μM) being the most potent tubulin polymerization inhibitor among the new compounds.

*3.2. MCF-7 breast cancer cell growth*

Several new indole derivatives inhibited the growth of human MCF-7 nonmetastatic breast cancer epithelial cells with $IC_{50}$ values at nanomolar concentrations (Table 1). Structure-activity relationship (SAR) analysis show three distinct groups: (i) introduction of the heterocyclic ring at position 5 of the indole had a relatively weak effect on inhibition of MCF-7 cell growth, with $IC_{50}$ values ranging from 70 (**3**) to 200 nM (**4**, **6**); (ii) compounds **7-14**, bearing the heterocyclic ring at position 6 of the indole, all were highly potent MCF-7 cell growth inhibitors, with $IC_{50}$ values ranging from 4.3 (**10**) to 18 (**14**) nM, with five compounds (**8** and **10-13**) having single digit nanomolar $IC_{50}$ values; (iii) the indoles with the heterocycle at position 7 showed different behavior, depending on the bridging group: the 7-heterocyclyl-3-arylthio-1*H*-indoles **15**, **17**, **19**

and **21** ($IC_{50}$s ranging from 15 to 38 nM) were more than one order of magnitude superior to the corresponding aroyl derivatives **16**, **18**, **20** and **22**.

A SAR summary of tubulin polymerization inhibition and inhibition of MCF-7 cell growth of compounds **3-22** is depicted in Chart 2. It should be noted that the SARs differ from those of the 2-phenyl-1*H*-indoles [27]. Compounds **3-6** with the heterocyclic ring at position 5 showed moderate inhibition of MCF-7 cell growth; compounds **7-14**, bearing the heterocycle at position 6 of the indole, all were potent MCF-7 cell growth inhibitors and showed comparable $IC_{50}$ values; derivatives **15**, **17**, **19** and **22**, with the heterocyclic ring at position 7 and the sulfur atom bridging the two aromatic ring systems, were substantially superior to the corresponding aroyl compounds (**16**, **18**, **20** and **22**).

*3.3. Inhibition of the binding of [$^3$H]colchicine to tubulin*

Compounds **3-22** were also examined for potential inhibition of the binding of [$^3$H]colchicine to tubulin (Table 1). Thirteen compounds, **3**, **5**, **7-17**, and **19** yielded >75% inhibition of the binding reaction. Interestingly, all the indoles with the heterocycle at position 7 were strong inhibitors of [$^3$H]colchicine binding, with **7** and **13** (97% inhibition) nearly as potent as CSA4 (98% inhibition). In general, good correlation between [$^3$H]colchicine binding and MCF-7 cell growth inhibition was observed: compounds which inhibited [$^3$H]colchicine binding >90%, inhibited the growth of the MCF-7 cancer cell with $IC_{50}$s ≤15 nM; compounds with 80-90% inhibition of [$^3$H]colchicine binding inhibited the growth of the MCF-7 cancer cell line with $IC_{50}$s in the range of 24-70 nM; except for **21**, compounds with 70-80% inhibition of [$^3$H]colchicine binding inhibited the growth of the MCF-7 cancer cells with $IC_{50}$s in the range of 150-350 nM.

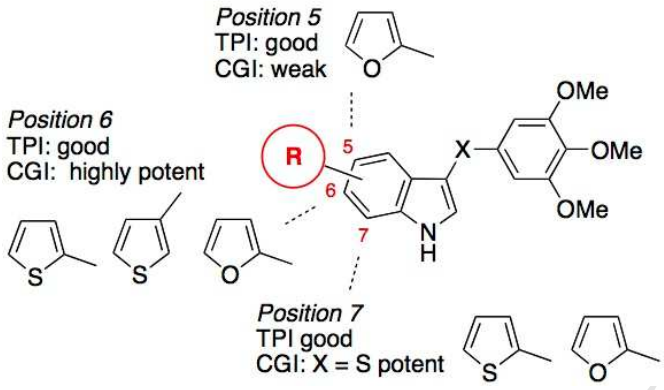


**Chart 2.** SAR summary for tubulin polymerization inhibition (TPI) and MCF-7 cell growth inhibition (CGI) by compounds **3-22**.

*3.4. Molecular modeling studies*

Compounds **6**, **13** and **19**, representative members of the heterocyclic substitutions at position 5-, 6- or 7- of the indole nucleus, were docked into the tubulin-DAMA-colchicine complex (PDB code 1SA0) [8] by following our previously reported procedure [30]. The docking studies were also performed for five newly available tubulin crystal structures [31]. The docking results in the different tubulin structures revealed a consistent binding mode for compounds bearing the heterocyclic ring at position 5-, 6- or 7- of the indole: (i) the 3,4,5-trimethoxyphenyl moiety formed an H-bond with the Cys241β side chain and hydrophobic contacts with Leu248β and Leu255β; (ii) the indole established hydrophobic contacts with Asn258β and Met259β; (iii) the heterocyclic ring of **6**, **13** and **19** at position 5, 6 or 7 of the indole, respectively, arranged hydrophobic interactions with Met259β, Lys353β, Ala180α and Val181 in the same cleft of the colchicine site (Figs. 1 and 2).

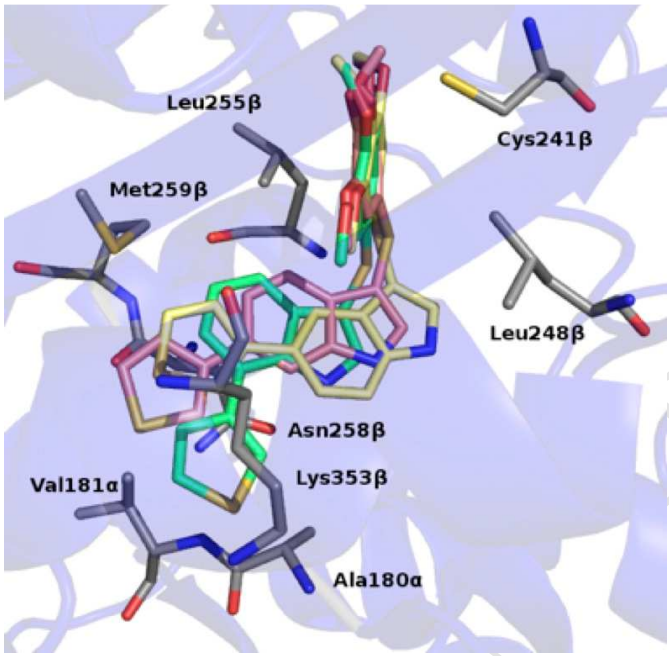


**Fig. 1.** Plants proposed binding mode for derivatives **6** (yellow), **19** (pink) and **21** (green) into the 1SA0 tubulin structure. Residues involved in interactions are shown as stick diagrams. The tubulin polypeptide chains are shown as ribbon cartoons.

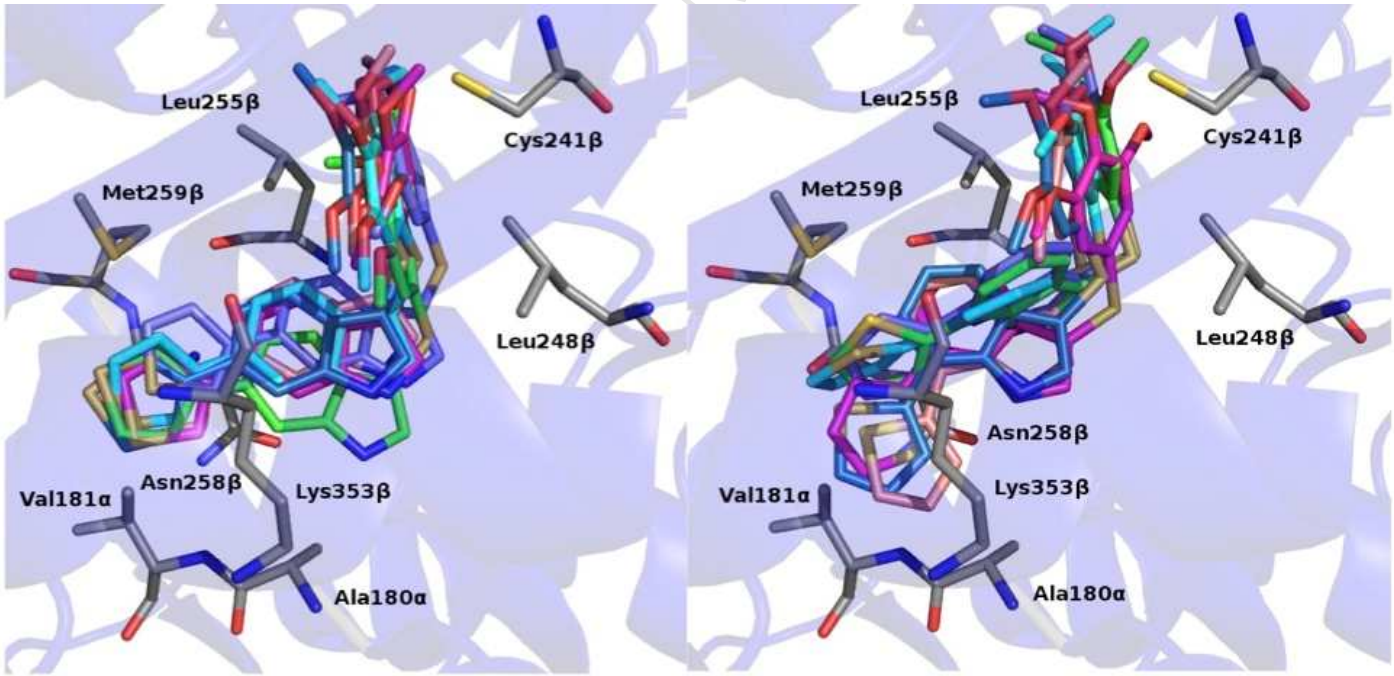


**Fig. 2.** Plants proposed binding mode for derivatives **13** (left panel) and **19** (right panel) for the studied tubulin structures: 1SA0 (green), 3HKC (cyan), 4O2B (magenta), 5CA0 (purple), 5CB4 (sky blue), 5LYJ (pink). Residues involved in interactions are shown as stick diagrams. The tubulin polypeptide chains are shown as ribbon cartoons. Residues and cartoon are from 1SA0.

### *3.5. Inhibition of growth of glioblastoma T98G, U87MG and U343MG cell lines*

Treatments of T98G (human glioblastoma), U87MG (human glioblastoma-astrocytoma) and U343MG (human glioblastoma-astrocytoma) cells with increasing concentrations of **13** and **19** significantly inhibited cell growth in a dose-dependent manner (Table 2 and Figs. 1SD-3SD, supplementary data). The $IC_{50}$ values were calculated taking into account the relative cellular doubling times [32,33] of 48 h for the T98G and U87MG cells and of 72 h for the U343MG cells. Compound **13** potently inhibited the glioblastoma cells at nanomolar concentrations. Arylthioindoles with the imidazol-1-yl or pyridin-4-yl heterocyclic ring at position 2 of the indole were weaker inhibitors of glioblastoma U87MG cells than were **13** and **19,** even though such compounds exhibited potent inhibition of the MCF-7 cancer cell growth [26].

### *3.6. Inhibition of HT29, HCT116 and HepG2 cancer cell growth*

Compounds **13** and **19** were evaluated as growth inhibitors of the human cell lines HT29 (colon adenocarcinoma), HCT116 (colon carcinoma), and HepG2 (hepatocellular carcinoma) using PTX as reference compound (Table 2). Compounds **13** and **19** showed strong inhibition of the HT29 and HCT116 cell lines. As inhibitors of the HepG2 cells, **13** and **19** were more effective than PTX ($IC_{50}$ = 2660 nM).

### *3.7. Inhibition of MV4-11, THP-1, A-549 and PC3 cell lines*

Compounds **13** and **19** were evaluated as inhibitors of MV4-11 (leukemia, acute myeloid), THP1 (leukemia, acute monocytic), A549 (lung carcinoma) and PC3 (prostate carcinoma) cancer cells. Compound **13** inhibited MV4-11, THP-1, A-549 and PC3 cells at single digit nanomolar concentration, while **19** was consistently less active (Table 2).

**Table 2**
Growth Inhibition of HT29, HCT116, HepG2, T98G, U87MG, U343G, MV4-11, THP-1, A-549 and PC3 cells by **13** and **19**.[a,b]

| Compd | $IC_{50}$ ± SD (nM) | | | | | | | | | |
|---|---|---|---|---|---|---|---|---|---|---|
| | HT29 | HCT116 | HepG2 | T98G | U87MG | U343G | MV4-11 | THP-1 | A-549 | PC3 |
| **13** | 10 ± 1.4 | 21 ± 1.5 | 20 ± 1.1 | 26 ± 3.6 | 16 ± 2.0 | 31 ± 4.3 | 6 ± 2.0 | 2 ± 1 | 2 ± 0.1 | 3.5 ± 2 |
| **19** | 69 ± 1.4 | 70 ± 1.7 | 80 ± 1.2 | 211 ± 20 | 96 ± 14 | 154 ± 6.9 | 70 ± 16 | 20 ± 2 | 58 ± 1 | 39 ± 4 |

[a] Cytotoxic concentrations for the indicated cell lines; cytostatic concentrations for A-549 and PC3 cells.
[b] Incubation time was 48 h; for U343G, MV4-11 and PC3 cells, incubation was 72 h.

### *3.8. MDR cell lines*

Compounds **13** and **19**, representative of the 6- and 7-heterocyclyl series, respectively, were compared with CSA4, VRB, VLB and PTX in the ovarian carcinoma cell lines OVCAR-8 and its cognate Pgp overexpressing line NCI/ADR-RES (Table 3). In contrast to CSA4, the standard agents VRB, VLB and PTX showed weak inhibition of the MDR line NCI/ADR-RES. The $IC_{50}$ values of **13** and **19** for the MCF-7 cells, repeated in this study, resembled those obtained in the studies summarized in Table 1.

**Table 3**
Growth Inhibition of the OVCAR-8 and NCI/ADR-RES cells by compounds **13** and **19** and reference compounds CSA4, VRB, VLB and PTX.[a]

| Compd | $IC_{50}$ ± SD (nM) | | |
|---|---|---|---|
| | OVCAR-8 | NCI/ADR_RES | MCF-7 |
| **13** | 9.3 ± 2 | 7.5 ± 2 | 6.7 ± 2 |
| **19** | 58 ± 8 | 34 ± 8 | 55 ± 7 |
| CSA4 | 4.0 ± 0[b] | 3.5 ± 0.7 | 5.0 ± 1 |
| PTX | 4.0 ± 1 | 3100 ± 600 | 5.5 ± 0.7 |
| VRB | 300 ± 0 | 5000 ± 1000 | Nd[c] |
| VBL | 15 ± 7 | 200 ± 0 | Nd |

[a] Inhibition of growth of the indicated cell lines.
[b] Same value obtained in all experiments. [c]Nd, not done.

*3.9. Compounds **13** and **19** induce cell cycle arrest in the G2/M phase in HeLa cells*

We compared cell cycle progression in HeLa cells exposed to 20, 50 and 100 nM **13** and **19**, using 20 nM VBL as a reference compound (a concentration that effectively arrests cells in mitosis [27]) and DMSO as a control. Cells were treated for 24 h to cover the average duration of an entire cell cycle, then harvested, incubated with propidium iodide (PI) and analyzed for their genomic content by FACS analysis. Representative cell cycle profiles are shown in Fig. 3A, left panel; data from three experiments are quantified in the graph in Fig. 3A, right panel. Both molecules inhibited cell cycle progression in a dose-dependent manner but with different effectiveness: treatment with 100 nM **19** yielded a substantial fraction (over 71%) of the cell population in the G2/M phase, whereas lower doses had no significant effect; compound **13** was already partly effective at 20 nM and induced substantial G2/M arrest at 50 nM (77% arrest).

Immunofluorescence (IF) analysis of **13** and **19**-treated HeLa cell cultures confirmed that treatment with 20 nM **13** (24 h) induced arrest in mitosis in over 50% of all cells, similar to the effect of VBL. The mitotic arrest was stable, and only 15% of the cell population included multinucleated cells, resulting from mitotic "slippage" and interphase re-entry with unsegregated, or randomly segregating, chromosomes. Compound **19** induced mitotic arrest with lower effectiveness than **13**: (i) 100 nM **19** arrested 50% of the cell population in mitosis, compared with 20 nM **13** or VBL; (ii) the induction of mitotic arrest by **19** was not fully sustained. The higher accumulation of cells in mitosis observed with 100 nM **19** was accompanied by induction of a relevant fraction (around 32%) of multinucleated cells: this suggests that cells that reached mitosis arrested only transiently, and eventually resumed mitotic progression with an inefficient mitotic apparatus, generating multinucleated cellular offspring (Fig. 3B).

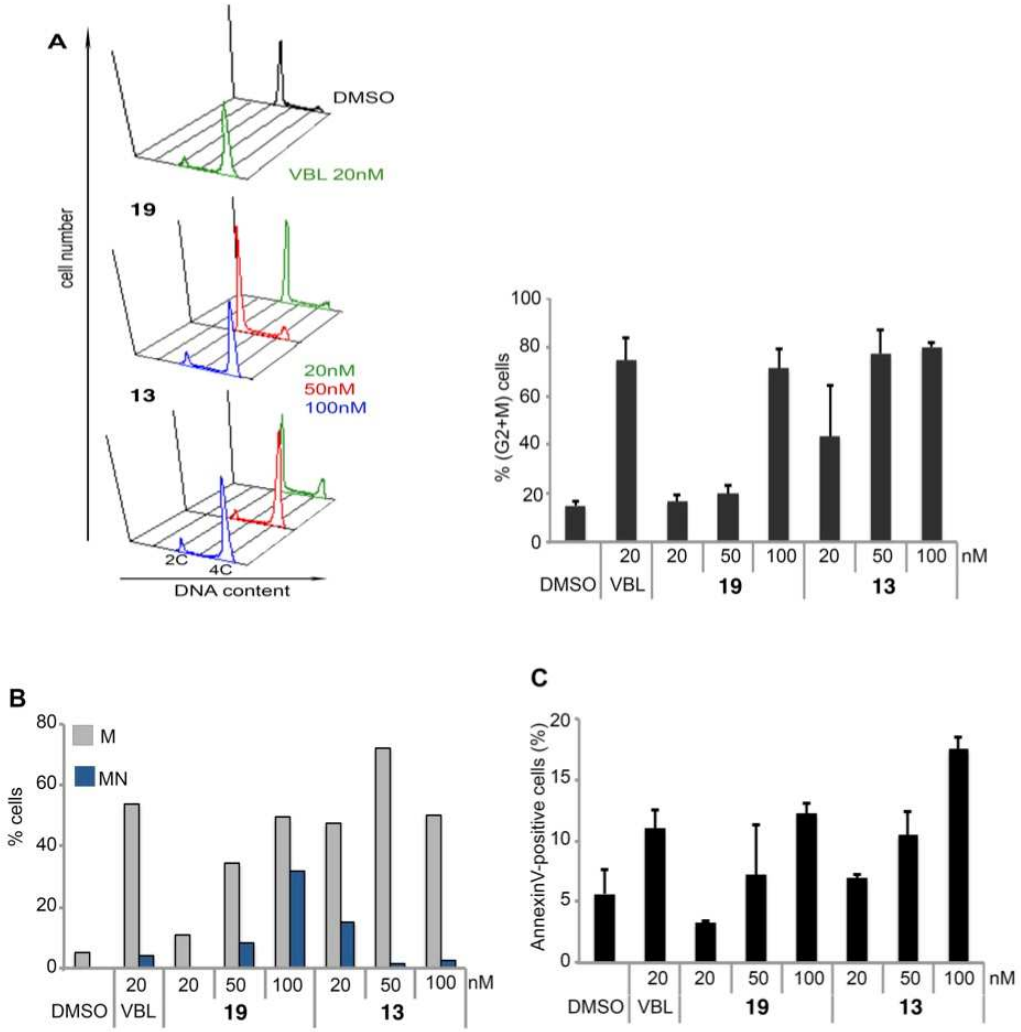


**Fig. 3.** FACS analysis of the cell cycle and cell death in HeLa cell populations treated with **13** or **19**. Panel A left: distribution of cells after a 24 h treatment with **13** or **19** or VBL (DMSO as control). The DNA content indicates the cell cycle phase (2C: G1; 4C: G2+M; intermediate values between 2C and 4C: S phase). The panel shows a representative analysis of the cell cycle phase distribution, arranged according to the compound concentration (on the *z* axis). In the lower two diagrams, 20 nM, green curves; 50 nM, red curves; 100 nM; blue curves. The profiles illustrate that **19** only induces 4C cell accumulation when used at 100 nM, whereas **13** is fully effective at 50 nM. Panel A right: the histograms show the mean % values ± SD of 4C cells (G2+M phases) counted in 3 independent experiments. Panel B: the graph represents the frequency of mitotic figures (grey bars) and multinucleated cells (blue bars) in cell populations treated for 24 h under the indicated conditions, processed for immunofluorescence and scored by microscopy. Between 300 and 650 cells were counted for each condition in 2 independent experiments. Panel C: FACS analysis of cell populations treated for 24 h under the indicated conditions and stained with annexin V. Mean ± SD values were calculated from three experiments.

We wondered whether cell cycle arrest by **13** and **19** was paralleled by cell death induction, as is the case with classical MT-targeting drugs. Cultures treated for 24 h were incubated with annexin V to identify cells with damaged plasma membranes committed to death. Both compounds activated cell death parallel to arresting cell cycle progression; again, **19** was effective when used at 100 nM, whereas 20 nM **13** was already partly effective and reached the same death-inducing capacity as VBL at the 50 nM dose (Fig. 3C).

The tubulin inhibitory effects of **13** and **19** at the cytological level were evaluated by IF analysis (Fig. 4). These assays provided a visual demonstration of the differential effectiveness of the two compunds. Compund **19** at 20 or 50 nM induced a mixture of apparently normal, or fragmented or multipolar spindles in variable proportions (examples are shown in Fig. 4A, phenotypes are quantified in Fig. 4C); 100 nM **19** largely induced small formations of radially arranged short microtubules that failed to elongate (labeled as “MT asters”, Fig. 4A, central row). Compound **13** had a more pronounced effect at all tested concentrations, and no cell showed a normal or only weakly affected spindle. Even with **13** at 20 nM, most mitotic cells displayed multipolar (Fig. 4B, top row) or fragmented spindles (Fig. 4B, central row); at higher concentration, 50 nM or above, **13** inhibited MT formation altogether, with sparse tubulin foci in virtually all treated cells (Fig. 4B, bottom row). Representative phenotypes are shown in Fig. 4A,B and quantified in Fig. 4C.

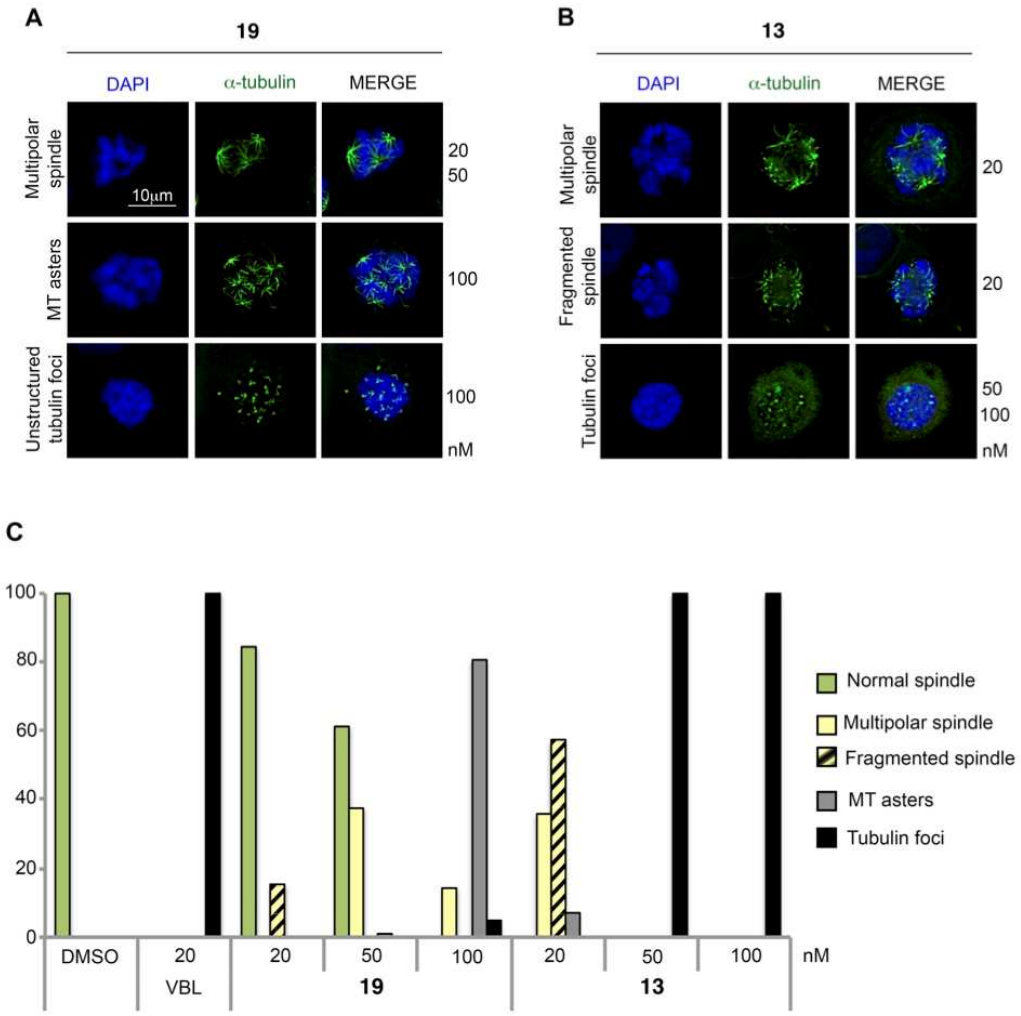


**Fig. 4.** IF analysis of mitotic cells in HeLa cultures treated with **13** or **19**. Panel A: representative phenotypes induced by **19**: all cells were arrested in prometaphase (compare the configuration of chromosomes in DAPI panels); the green channel shows the extent of inhibition of tubulin polymerization at increasing compound concentrations (indicated at the right of the panels in nM). Panel B: representative phenotypes induced by **13**: the DAPI panels show the prometaphase configuration of chromosomes; the green channel shows the extent of inhibition of tubulin polymerization at the indicated concentrations. Panel C: Distribution of tubulin cytological phenotypes under the indicated conditions. The histograms represent the frequency of the indicated phenotypes (n, 100 to 250 prometaphase-arrested cells per condition).

In summary, both **13** and **19** arrested cells in mitosis, with formation of a defective mitotic apparatus, yet the two compounds showed differential effectiveness. Compound **13** induced the

inhibition of MT polymerization to a greater extent than **19**, and it showed a full inhibitory effect on tubulin polymerization in cells at 50 nM, comparable to the effect of VBL. Compound **19** induced milder inhibition: it essentially affected the mitotic spindle structural organization but did not fully inhibit tubulin polymerization in cells below 100 nM. The parallel observation that **13** was a more effective inducer of cell death than **19** correlated with cellular data on microtubule disruption and with inhibition of [$^3$H]colchicine binding.

*3.10. Effects of **13** or **19** on viability of HepG2 cells*

HepG2 cells were treated with different concentrations of **13** or **19** and analyzed by the MTT assay. Treatment with compound **19** for 48 h caused a dose-dependent decrease of cell viability: at 80 nM nearly 30% of cells displayed reduced viability as compared to untreated cells (Fig. 4SD, panel A, supplementary data). The dose-dependent decrease of cell viability on treatment with **13** became significant at 20 nM, nearly 40% of cells were affected (Fig. 4SD, panel B, supplementary data). These experiments indicated 80 nM **19** and 20 nM **13** are optimal concentrations to induce significant modifications in cell viability but, at the same time, preserving a sufficient proportion of the cell population to permit further analysis. At such concentrations, **13** and **19** caused a marked impairment of HepG2 cell growth after a 48 h treatment. The cell-cycle blocker $p21^{Cip1/Waf1}$ was significantly up-regulated in HepG2 treated cells at these doses. After 80 nM **19** (Fig. 5SD, panel A, supplementary data) or 20 nM **13** (Fig. 5SD, panel B, supplementary data) treatments, the transcript levels of $p21^{Cip1/Waf1}$, assessed by qRT-PCR, were increased by 1.5- and 3.9-fold, respectively, as compared with untreated cells.

*3.11. Evaluation of the drug-like properties of **13** and **19***

Drug like properties of compounds **13** and **19** were predicted through the most common descriptors of drug-likeness (Table 4). Oral absorption according to Lipinski's rule of five [34] and Veber's rule [35] was estimated by FAF drug server [36]. We referred to the 3/75 rule (logP > 3 and topological PSA < 75 $Å^2$) [37] to estimate compound toxicity. Derivatives **13** and **19** properly fitted with both Lipinsky and Veber's rules, suggesting a potential good absorption after oral administration. Furthermore, a low likelihood of in vivo toxicological outcome was inferred by the 3/75 rule (Fig. 5).

**Table 4**
Physico-chemical profiles of compounds **13** and **19**

| Compd | LogP[a] | MW[b] | LogSw[c] | tPSA[d] | HBA-HBD[e] | RoF viol[f] | Veber[g] | 3/75[h] |
|---|---|---|---|---|---|---|---|---|
| **13** | 5.34 | 397.51 | -5.58 | 97.02 | 5 | 1 | good | warning |
| **19** | 5.37 | 397.51 | -5.60 | 97.02 | 5 | 1 | good | warning |

[a] Logarithm of the partition coefficient between *n*-octanol and water computed by XLOGP3 method [38].
[b] Molecular weight.
[c] LogSw represents the logarithm of compound water solubility computed by the ESOL method [39].
[d] Molecular polar surface area, this parameter has been shown to correlate with human intestinal absorption (<140) [40].
[e] Number H-bond acceptors and H-bond donors.
[f] Violation of the rule of five [34].
[g] Veber's rule matching [35].
[h] 3/75 rule matching [36].

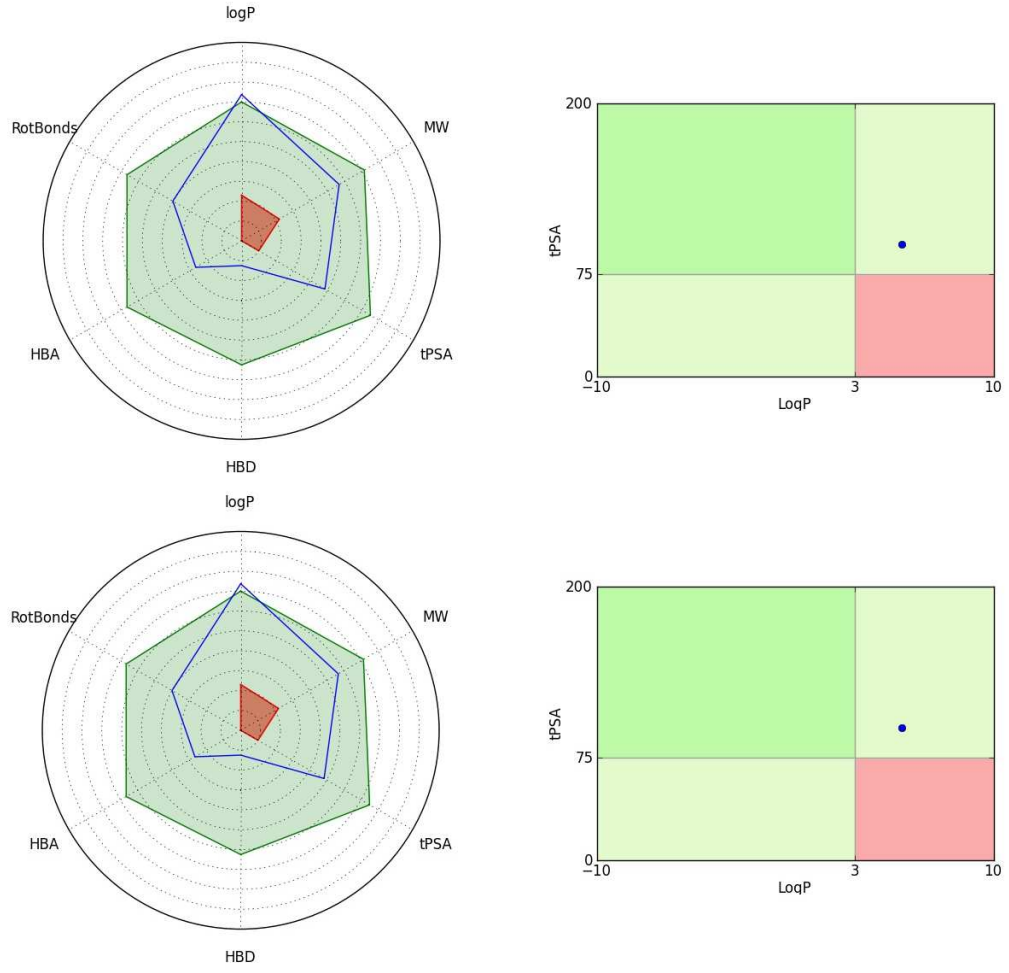


**Fig. 5.** Physico-chemical properties. Panel A. Compounds **13** and **19** (blue lines) are compared with the optimal light green area defined by Lipinski's rule-of-five and Veber's rule. The computations includes logP, molecular weight (MW), topological polar surface area (tPSA), rotatable bonds (RotB), H-bond acceptors and donors (HBA, HBD. The red area indicates low oral bioavailability. Estimated physico-chemical profiles of compounds **13** and **19** fall within the light green area. Panel B. Likelihood of in vivo toxicity according 3/75 rule [37]. tPSA is expressed as a function of logP. Compounds located in the red square are likely to cause toxicity. Estimated toxicities of compounds **13** and **19** (blues point) fall within the light green area.

## 4. Conclusions

We designed new 3-arylthio- and 3-aroyl-1*H*-indole derivatives **3-22** bearing a heterocyclic ring at position 5, 6 or 7 of the indole nucleus. Ten new derivatives inhibited polymerization of

purified tubulin with $IC_{50}$ values at submicromolar concentrations. Seven of the new indole derivatives inhibited the growth of MCF-7 cells with $IC_{50}$ values ≤10 nM. Inhibition of cell growth showed good correlation with inhibition of [$^3$H]colchicine binding to tubulin. Two representative highly potent members of the 6- and 7-heterocyclyl-1*H*-indoles, **13** and **19**, inhibited an extensive panel of cancer cell lines, including the Pgp overexpressing NCI/ADR-RES cell line, with nanomolar $IC_{50}$s. In cell cycle analysis, compound **13** became effective at 20 nM and induced 77% G2/M arrest at 50 nM, whereas **19** accumulated 71% cells in the G2/M phase at 100 nM. Compound **13** extensively inhibited cellular tubulin polymerization at 50 nM, and its activity was comparable to that of VBL. Compound **19** at 100 nM affected mitotic spindle structural organization but did not fully inhibit cellular tubulin polymerization. As inhibitors of HepG2 cells, **13** and **19** ($IC_{50}$ values of 20 nM and 80 nM, respectively) were distinctly superior to PTX. Compound **13** was also a potent inhibitor of the U87MG glioblastoma cell line at nanomolar concentrations [41] being almost one order of magnitude more active than the previously reported arylthioindoles with the imidazol-1-yl or pyridin-4-yl ring at position 2 of the indole nucleus [26]. Analysis of the gene expression levels of $p21^{Cip1/Waf1}$, the cell cycle blocker, indicated that at sub-cytotoxic concentrations **13** caused a decrease in cell growth with strong up-regulation of $p21^{Cip1/Waf1}$ [42].

In conclusion, these new indoles are potent inhibitors of tubulin polymerization and cancer cell growth, including human liver carcinoma and glioblastoma cells. The introduction of the heterocyclic ring at position 5, 6 or 7 of the 3-(3',4',5'-trimethoxyarylthio)-1*H*-indole and 3-(3',4',5'-trimethoxyaroyl)-1*H*-indole scaffold was a productive strategy for the design of new effective anticancer agents, with compound **13** as a robust lead agent. Based on SAR findings,

the synthesis of new analogues is in progress in our laboratory, and the results will be reported in due course.

## 5. Experimental protocols

### *5.1. Chemistry*

All reagents and solvents were handled according to the material safety data sheet of the supplier and were used as purchased without further purification. 5-Chloro-1*H*-indole (**23**), 5-iodo-1*H*-indole (**24**), 6-bromo-1*H*-indole (**25**), 7-iodo-1*H*-indole (**26**), 6-(thiophen-2-yl)-1*H*-indole (**33**) and 6-(thiophen-3-yl)-1*H*-indole (**34**) were commercially available. MW-assisted reactions were performed on a CEM Discover SP single-mode reactor equipped with an Explorer 72 autosampler, controlling the instrument settings by PC-running CEM Synergy 1.60 software. Closed vessel experiments were carried out in capped MW-dedicated vials (10 mL) with a cylindrical stirring bar (length 8 mm, diameter 3 mm). Stirring, temperature, irradiation power, maximum pressure (Pmax), pressure set point, times at set point, delta pressure, PowerMAX (simultaneous cooling-while-heating), ActiVent (simultaneous venting-while-heating), and ramp and hold times were set as indicated. Reaction temperature was monitored by an external CEM fiber optic temperature sensor. After completion of the reaction, the mixture was cooled to 25 °C via air-jet cooling. Organic solutions were dried over anhydrous sodium sulfate. Evaporation of solvents was carried out on a Büchi Rotavapor R-210 equipped with a Büchi V-850 vacuum controller and a Büchi V-700 vacuum pump. Column chromatography was performed on columns packed with silica gel from Macherey-Nagel (70−230 mesh). Silica gel thin layer chromatography (TLC) cards from Macherey-Nagel (silica gel precoated aluminum cards with fluorescent indicator visualizable at 254 nm) were used for TLC. Developed plates were visualized with a Spectroline ENF 260C/FE UV apparatus. Melting points (mp) were determined

on a Stuart Scientific SMP1 apparatus and are uncorrected. Infrared (IR) spectra were recorded on a PerkinElmer Spectrum 100 FT-IR spectrophotometer equipped with a universal attenuated total reflectance accessory and IR data acquired and processed by PerkinElmer Spectrum 10.03.00.0069 software. Band position and absorption ranges are given in $cm^{-1}$. Proton nuclear magnetic resonance ($^1H$ NMR) spectra were recorded with a Varian Mercury (300 MHz) or a Bruker Avance (400 MHz) spectrometer in the indicated solvent, and the corresponding fid files were processed by MestreLab Research SL MestreReNova 6.2.1-769 software. Chemical shifts are expressed in δ units (ppm) from tetramethylsilane. Mass spectra were recorded on a Bruker Daltonics MicroTOF LC/MS mass spectrometer equipped with a positive ion ESI source. Compound purity was checked by high pressure liquid chromatography (HPLC). Purity of tested compounds was found to be >95%. The HPLC system used (Thermo Fisher Scientific Inc. Dionex UltiMate 3000) consisted of an SR-3000 solvent rack, a LPG-3400SD quaternary analytical pump, a TCC-3000SD column compartment, a DAD-3000 diode array detector, and an analytical manual injection valve with a 20 μL loop. Samples were dissolved in acetonitrile (1 mg/mL). HPLC analysis was performed by using a Thermo Fisher Scientific Inc. Acclaim 120 C18 column (5 μm, 4.6 mm × 250 mm) at 25 ± 1 °C with an appropriate solvent gradient (acetonitrile/water), flow rate of 1.0 mL/min and signal detector at 206, 230, 254 and 365 nm. Chromatographic data were acquired and processed by Thermo Fisher Scientific Inc. Chromeleon 6.80 SR15 Build 4656 software.

*5.1.1. General procedure for the synthesis of derivatives **3-7**, **9**, **11**, **13**, **15**, **19** and **37**. Example. 5-(Furan-2-yl)-3-((3,4,5-trimethoxyphenyl)thio)-1H-indole (**3**)*

A mixture of indole **27** (183 mg, 1 mmol), bis(3,4,5-trimethoxyphenyl)disulfide [29] (438 mg, 1.1 mmol), and sodium hydride (88 mg, 2.2 mmol; 60% in mineral oil) in anhydrous DMF (3

mL) was placed into the MW cavity (closed vessel mode, Pmax = 250 psi). Starting MW irradiation of 120 W was used, the temperature being ramped from 25 to 130 °C, while rapidly stirring and venting (pressure set point: 100 psi; times at set point: 100; delta pressure: 20 psi). Once 130 °C was reached, taking about 1 min, the reaction mixture was held at this temperature for 2 min. The mixture was diluted with water and extracted with ethyl acetate. The organic layer was washed with brine and dried. Removal of the solvent gave a residue that was purified by column chromatography (silica gel, *n*-hexane:ethyl acetate = 3:2 as eluent) to give **3** (122 mg, yield 32%), mp 118-120 °C (from ethanol). $^1$H NMR (DMSO-$d_6$, 400 MHz): $\delta$ 3.98 (s, 9H), 6.82 (s, 2H), 6.95 (s, 1H), 7.22 (d, $J$ = 1.7 Hz, 1H), 7.93-7.96 (m, 2H), 8.07 (s, 1H), 8.17 (s, 1H), 8.22 (s, 1H), 12.20 ppm (br s, disappeared after treatment with $D_2O$, 1H). IR: $v$ 3448 cm$^{-1}$. MS (ESI): 382.4 ($MH^+$). $C_{21}H_{19}NO_4S$ (381.45).

*5.1.2. 5-(Furan-3-yl)-3-((3,4,5-trimethoxyphenyl)thio)-1H-indole (**4**)*

Synthesized as **3** starting from **28**. Yield 20%, mp 125-130 °C (from ethanol). $^1$H NMR (DMSO-$d_6$, 400 MHz): $\delta$ 3.57 (s, 3H), 3.59 (s, 6H), 6.44 (s, 2H), 6.89-6.91 (m, 1H), 7.45-7.47 (m, 2H), 7.61-7.65 (m, 1H), 7.70 (d, $J$ = 1.7 Hz, 1H), 7.77 (s, 1H), 8.05-8.10 (m, 1H), 11.70 ppm (br s, disappeared after treatment with $D_2O$, 1H). IR: $v$ 3425 cm$^{-1}$. MS (ESI): 382.2 ($MH^+$). $C_{21}H_{19}NO_4S$ (381.45).

*5.1.3. 5-(Thiophen-2-yl)-3-((3,4,5-trimethoxyphenyl)thio)-1H-indole (**5**)*

Synthesized as **3** starting from **29**. Yield 31%, mp 115-120 °C (from ethanol). $^1$H NMR ($CDCl_3$, 400 MHz): $\delta$ 3.69 (s, 6H), 3.78 (s, 3H), 6.44 (s, 2H), 7.00-7.07 (m, 1H), 7.24 (dd, $J$ = 2.9 and 7.1 Hz, 1H), 7.28 (s, 1H), 7.44 (d, $J$ = 8.5 Hz, 1H), 7.52 (d, $J$ = 2.6 Hz, 1H), 7.55-7.60 (m, 1H), 7.89 (s, 1H), 8.49 ppm (br s, disappeared after treatment with $D_2O$, 1H). IR: $v$ 3439 cm$^{-1}$. MS (ESI): 398.4 ($MH^+$). $C_{21}H_{19}NO_3S_2$ (397.51).

*5.1.4. 5-(Thiophen-3-yl)-3-((3,4,5-trimethoxyphenyl)thio)-1H-indole (**6**)*

Synthesized as **3** starting from **30**. Yield 40%, mp 116-120 °C (from ethanol). $^1$H NMR (DMSO-$d_6$, 400 MHz): $\delta$ 3.57 (s, 3H), 3.58 (s, 6H), 6.44 (s, 2H), 7.49-7.51 (m, 1H), 7.53 (s, 1H), 7.55 (d, $J$ = 1.3 Hz, 1H), 7.59-7.62 (m, 1H), 7.72-7.74 (m, 2H), 7.79 (d, $J$ = 2.4 Hz, 1H), 11.71 ppm (br s, disappeared after treatment with $D_2O$, 1H). IR: $\nu$ 3448 cm$^{-1}$. MS (ESI): 398.5 ($MH^+$). $C_{21}H_{19}NO_3S_2$ (397.51).

*5.1.5. 6-(Furan-2-yl)-3-((3,4,5-trimethoxyphenyl)thio)-1H-indole (**7**)*

Synthesized as **3** starting from **31**. Yield 44%, mp 164-169 °C (from ethanol). $^1$H NMR (DMSO-$d_6$, 300 MHz): $\delta$ 3.56 (s, 9H), 6.37 (s, 2H), 6.56-6.60 (m, 1H), 6.85 (d, $J$ = 3.2 Hz, 1H), 7.45 (s, 2H), 7.70-7.74 (m, 3H), 11.74 ppm (br s, disappeared after treatment with $D_2O$, 1H). IR: $\nu$ 3179 cm$^{-1}$. MS (ESI): 382.2 ($MH^+$). $C_{21}H_{19}NO_4S$ (381.45).

*5.1.6. 6-(Furan-3-yl)-3-((3,4,5-trimethoxyphenyl)thio)-1H-indole (**9**)*

Synthesized as **3** starting from **32**. Yield 4%, slurry. $^1$H NMR (DMSO-$d_6$, 400 MHz): $\delta$ 3.57 (s, 9H), 6.39 (s, 2H), 6.90-6.95 (m, 1H), 7.34-7.36 (m, 1H), 7.40-7.43 (m, 1H), 7.63 (s, 1H), 7.70-7.73 (m, 2H), 8.14 (s, 1H), 11.66 ppm (br s, disappeared after treatment with $D_2O$, 1H). IR: $\nu$ 3401 cm$^{-1}$. MS (ESI): 382.2 ($MH^+$). $C_{21}H_{19}NO_4S$ (381.45).

*5.1.7. 6-(Thiophen-2-yl)-3-((3,4,5-trimethoxyphenyl)thio)-1H-indole (**11**)*

Synthesized as **3** starting from **33**. Yield 50%, mp 158-161 °C (from ethanol). $^1$H NMR (DMSO-$d_6$, 400 MHz): $\delta$ 3.58 (s, 3H), 3.59 (s, 6H), 6.41 (s, 2H), 7.10-7.13 (m, 1H), 7.41-7.43 (m, 1H), 7.44-7.48 (m, 3H), 7.70-7.72 (m, 1H), 7.82 (s, 1H), 11.74 ppm (br s, disappeared after treatment with $D_2O$, 1H). IR: $\nu$ 3372 cm$^{-1}$. MS (ESI): 398.3 ($MH^+$). $C_{21}H_{19}NO_3S_2$ (397.51).

*5.1.8. 6-(Thiophen-3-yl)-3-((3,4,5-trimethoxyphenyl)thio)-1H-indole (**13**)*

Synthesized as **3** starting from **39**. Yield 30%, mp 188-190 °C (from ethanol). $^1$H NMR (DMSO-$d_6$, 400 MHz): $\delta$ 3.58 (s, 3H), 3.59 (s, 6H), 6.40 (s, 2H), 7-45-7.47 (m, 2H), 7.52-7.57 (m, 1H), 7.60-7.64 (m, 1H), 7.76 (s, 1H), 7.79 (s, 1H), 7.77-7.81 (m, 1H), 11.72 ppm (br s, disappeared after treatment with $D_2O$, 1H). IR: $v$ 3376 cm$^{-1}$. MS (ESI): 398.5 ($MH^+$). $C_{21}H_{19}NO_3S_2$ (397.51).

*5.1.9. 7-(Furan-2-yl)-3-((3,4,5-trimethoxyphenyl)thio)-1H-indole (**15**)*

Synthesized as **3** starting from **35**. Yield 15%, mp 80-83 °C (from ethanol). $^1$H NMR (DMSO-$d_6$, 400 MHz): $\delta$ 3.58 (s, 9H), 6.42 (s, 2H), 6.71-6.75 (m, 1H), 7.16-7.21 (m, 2H), 7.44-7.50 (m, 1H), 7.59-7.63 (m, 1H), 7.80-7.83 (m, 2H), 11.59 ppm (br s, disappeared after treatment with $D_2O$, 1H). IR: $v$ 3351 cm$^{-1}$. MS (ESI): 382.2 ($MH^+$). $C_{21}H_{19}NO_4S$ (381.45).

*5.1.10. 7-(Thiophen-2-yl)-3-((3,4,5-trimethoxyphenyl)thio)-1H-indole (**19**)*

Synthesized as **3** starting from **36**. Yield 29%, mp 153-155 °C (from ethanol). $^1$H NMR (DMSO-$d_6$, 300 MHz): $\delta$ 3.56 (s, 3H), 3.58 (s, 6H), 6.43 (s, 2H), 7.14 (t, $J$ = 5.8 Hz, 1H), 7.24 (t, $J$ = 3.8 Hz, 1H), 7.32 (d, $J$ = 5.5 Hz, 1H), 7.46 (d, $J$ = 5.9 Hz, 1H), 7.56 (d, $J$ = 2.7 Hz, 1H), 7.64 (d, $J$ = 3.8 Hz, 1H), 7.76 (s, 1H), 11.57 ppm (br s, disappeared after treatment with $D_2O$, 1H). IR: $v$ 3322 cm$^{-1}$. MS (ESI): 398.4 ($MH^+$). $C_{21}H_{19}NO_3S_2$ (397.51).

*5.1.11. 7-Iodo-3-((3,4,5-trimethoxyphenyl)thio)-1H-indole (**37**)*

Synthesized as **3** starting from **26**. Yield 27%, mp 100-103 °C (from ethanol). $^1$H NMR (DMSO-$d_6$, 400 MHz): $\delta$ 3.56 (s, 3H), 3.57 (s, 6H), 6.40 (s, 2H), 6.90 (t, $J$ = 7.6 Hz, 1H), 7.46 (d, $J$ = 7.8 Hz, 1H), 7.58 (d, $J$ = 7.4 Hz, 1H), 7.77 (s, 1H), 11.61 ppm (br s, disappeared after treatment with $D_2O$, 1H). IR: $v$ 3270 cm$^{-1}$.

*5.1.12. General procedure for the synthesis of derivatives **8**, **10**, **12** and **14**. Example. (6-(Furan-2-yl)-1H-indol-3-yl)(3,4,5-trimethoxyphenyl)methanone (**8**).*

Diethylaluminum chloride (120 mg, 1 mmol; 1.0 M in hexanes) was added to a -78 °C solution of indole **31** (183 mg, 1 mmol) in dichloromethane (2.5 mL). The reaction mixture was warmed to -10 °C, and 3,4,5-trimethoxybenzoyl chloride (276 mg, 1.2 mmol) was added. The reaction mixture was stirred for 2 h, and the temperature rose to 25 °C. Water and chloroform were added, and the layers were separated. The organic phase was washed with brine, dried and filtered. Evaporation of the solvent gave a residue that was purified by column chromatography (silica gel, *n*-hexane:acetone = 7:3 as eluent) to give **8** (53 mg, yield 14%), mp 190-195 °C (from ethanol). $^1$H NMR (DMSO-$d_6$, 400 MHz): $\delta$ 3.75 (s, 3H), 3.85 (s, 6H), 6.58-6.62 (m, 1H), 6.88-6.92 (m, 1H), 7.10 (s, 2H), 7.61 (dd, $J$ = 1.4 and 8.4 Hz, 1H), 7.74-7.78 (m, 2H), 8.13 (s, 1H), 8.20-8.24 (m, 1H), 12.11 ppm (br s, disappeared after treatment with $D_2O$, 1H). IR: $\nu$ 1573 and 3192 cm$^{-1}$. MS (ESI): 378.4 ($MH^+$). $C_{22}H_{19}NO_5$ (377.40).

*5.1.13. (6-(Furan-3-yl)-1H-indol-3-yl)(3,4,5-trimethoxyphenyl)methanone (**10**)*

Synthesized as **8** starting from **32**. Yield 17%, mp 180-185 °C (from ethanol). $^1$H NMR (DMSO-$d_6$, 300 MHz): $\delta$ 3.75 (s, 3H), 3.85 (s, 6H), 6.95-6.98 (m, 1H), 7.09 (s, 2H), 7.50-7.55 (m, 1H), 7.66 (s, 1H), 7.75 (t, $J$ = 1.4 Hz, 1H), 8.07 (s, 1H), 8.18-8.20 (m, 2H), 12.04 ppm (br s, disappeared after treatment with $D_2O$, 1H). IR: $\nu$ 1576 and 3238 cm$^{-1}$. MS (ESI): 378.4 ($MH^+$). $C_{22}H_{19}NO_5$ (377.40).

*5.1.14. (6-(Thiophen-2-yl)-1H-indol-3-yl)(3,4,5-trimethoxyphenyl)methanone (**12**)*

Synthesized as **8** starting from **33**. Yield 68%, mp 200-205 °C (from ethanol). $^1$H NMR (DMSO-$d_6$, 300 MHz): $\delta$ 3.75 (s, 3H), 3.85 (s, 6H), 7.09 (s, 2H), 7.14-7.20 (m, 1H), 7.45-7.50 (m, 2H), 7.56 (dd, $J$ = 1.5 and 8.3 Hz, 1H), 7.73-7.76 (m, 1H), 8.12 (s, 1H), 8.23 (d, $J$ = 8.2 Hz,

1H), 12.04 ppm (br s, disappeared after treatment with $D_2O$, 1H). IR: *v* 1575 and 3219 $cm^{-1}$. MS (ESI): 394.4 ($MH^+$). $C_{22}H_{19}NO_4S$ (393.46).

*5.1.15. (6-(Thiophen-3-yl)-1H-indol-3-yl)(3,4,5-trimethoxyphenyl)methanone (**14**)*

Synthesized as **8** starting from **34**. Yield 69%, mp 188-192 °C (from ethanol). $^1H$ NMR (DMSO-$d_6$, 400 MHz): $\delta$ 3.74 (s, 3H), 3.84 (s, 6H), 7.08 (s, 2H), 7.60-7.65 (m, 3H), 7.72-7.76 (m, 1H), 7.82-7.85 (m, 1H), 8.10 (s, 1H), 8.22 (d, *J* = 8.3 Hz, 1H), 12.05 ppm (br s, disappeared after treatment with $D_2O$, 1H). IR: *v* 1733 and 3113 $cm^{-1}$. MS (ESI): 394.2 ($MH^+$). $C_{22}H_{19}NO_4S$ (393.46).

*5.1.16. General procedure for the synthesis of derivatives **16-18**, **20-22**, **30-32**, **35** and **36**. (7-(Furan-2-yl)-1H-indol-3-yl)(3,4,5-trimethoxyphenyl)methanone (**16**).*

A mixture of derivative **38** (437 mg, 1 mmol), tris(dibenzylideneacetone)dipalladium(0) (20 mg, 0.022 mmol), 2-dicyclohexylphosphino-2′,6′-dimethoxybiphenyl (3.2 mg, 0.008 mmol) and potassium phosphate tribasic (435 mg, 2.05 mmol) was degassed for 20 min. 1-Butanol (2.2 mL) and a solution of 2-furanylboronic acid MIDA ester (2-(furan-2-yl)-6-methyl-1,3,6,2-dioxazaborocane-4,8-dione) (334 mg, 1.5 mmol) in the same solvent (4.4 mL) were added. The reaction mixture was heated at 100 °C for 15 h. After cooling, the mixture was treated dropwise with 1 N HCl and extracted with ethyl acetate. The organic layer was washed with brine, dried and filtered. Evaporation of the solvent gave a residue that was purified by column chromatography (silica gel, *n*-hexane:acetone = 2:1 as eluent) to give **16** (124 mg, yield 33%), mp 221-224 °C (from ethanol). $^1H$ NMR (DMSO-$d_6$, 400 MHz): $\delta$ 3.76 (s, 3H), 3.85 (s, 6H), 6.71-6.75 (m, 1H), 7.12 (s, 2H), 7.15 (d, *J* = 3.4 Hz, 1H), 7.31 (t, *J* = 7.7 Hz, 1H), 7.63 (dd, *J* = 1.1 and 7.5 Hz, 1H), 7.80-7.85 (m, 1H), 7.98 (s, 1H), 8.23 (dd, *J* = 1.1 and 8.0 Hz, 1H), 11.85

ppm (br s, disappeared after treatment with $D_2O$, 1H). IR: *v* 1623 and 3427 $cm^{-1}$. MS (ESI): 378.3 ($MH^+$). $C_{22}H_{19}NO_5$ (377.40).

*5.1.17. 7-(Furan-3-yl)-3-((3,4,5-trimethoxyphenyl)thio)-1H-indole (**17**)*

Synthesized as **16** from **37** and furan-3-boronic acid pinacol ester. Yield 58%, mp 156-160 °C (from ethanol). $^1H$ NMR (DMSO-$d_6$, 400 MHz): $\delta$ 3.57 (s, 3H), 3.58 (s, 6H), 6.42 (s, 2H), 7.04 (m, 1H), 7.15 (t, *J* = 7.7 Hz, 1H), 7.40 (m, 2H), 7.78 (s, 1H), 7.85 (t, *J* = 1.8 Hz, 1H), 8.31 (t, *J* = 1.3 Hz, 1H), 11.39 ppm (br s, disappeared after treatment with $D_2O$, 1H). IR: *v* 3318 $cm^{-1}$. MS (ESI): 382.4 ($MH^+$). $C_{21}H_{19}NO_4S$ (381.45).

*5.1.18. (7-(Furan-3-yl)-1H-indol-3-yl)(3,4,5-trimethoxyphenyl)methanone (**18**)*

Synthesized as **16** starting from **38** and furan-3-boronic acid pinacol ester. Yield 46%, mp 215-220 °C (from ethanol). $^1H$ NMR (DMSO-$d_6$, 400 MHz): $\delta$ 3.76 (s, 3H), 3.85 (s, 6H), 7.00-7.05 (m, 1H), 7.11 (s, 2H), 7.29 (t, *J* = 7.9 Hz, 1H), 7.42 (dd, *J* = 1.1 and 7.4 Hz, 1H), 7.86 (t, *J* = 1.8 Hz, 1H), 7.97 (s, 1H), 8.21 (dd, *J* = 1.2 and 8.0 Hz, 1H), 8.25-8.30 (m, 1H), 11.76 ppm (br s, disappeared after treatment with $D_2O$, 1H). IR: *v* 1568 and 3285 $cm^{-1}$. MS (ESI): 378.4 ($MH^+$). $C_{22}H_{19}NO_5$ (377.40).

*5.1.19. (7-(Thiophen-2-yl)-1H-indol-3-yl)(3,4,5-trimethoxyphenyl)methanone (**20**)*

Synthesized as **16** starting from **38** and 2-thienylboronic acid. Yield 6%, mp 209-211 °C (from ethanol). $^1H$ NMR (DMSO-$d_6$, 400 MHz): $\delta$ 3.76 (s, 3H), 3.85 (s, 6H), 7.11 (s, 2H), 7.28-7.33 (m, 2H), 7.38 (dd, *J* = 1.2 and 7.4 Hz, 1H), 7.56 (dd, *J* = 1.2 and 3.6 Hz, 1H), 7.68 (dd, *J* = 1.1 and 5.1 Hz, 1H), 7.95 (s, 1H), 8.25 (dd, *J* = 1.2 and 7.9 Hz, 1H), 11.94 ppm (br s, disappeared after treatment with $D_2O$, 1H). IR: *v* 1573 and 3263 $cm^{-1}$. MS (ESI): 394.4 ($MH^+$). $C_{22}H_{19}NO_4S$ (393.46).

*5.1.20. 7-(Thiophen-3-yl)-3-((3,4,5-trimethoxyphenyl)thio)-1H-indole (**21**)*

Synthesized as **16** starting from **37** and 3-thienylboronic acid. Yield 75%, mp 147-150 °C (from ethanol). $^1$H NMR (DMSO-$d_6$, 400 MHz): $\delta$ 3.57 (s, 3H), 3.58 (s, 6H), 6.43 (s, 2H), 7.15 (t, $J$ = 7.8 Hz, 1H), 7.35 (dd, $J$ = 1.1 and 7.4 Hz, 1H), 7.44 (dd, $J$ = 1.1 and 7.9 Hz, 1H), 7.54 (dd, $J$ = 1.4 and 5.0 Hz, 1H), 7.70-7.75 (m, 2H), 7.80-7.85 (m, 1H), 11.52 ppm (br s, disappeared after treatment with $D_2O$, 1H). IR: $v$ 3327 cm$^{-1}$. MS (ESI): 398.4 ($MH^+$). $C_{21}H_{19}NO_3S_2$ (397.51).

*5.1.21. (7-(Thiophen-3-yl)-1H-indol-3-yl)(3,4,5-trimethoxyphenyl)methanone (**22**)*

Synthesized as **16** starting from **38** and 3-thienylboronic acid. Yield 5%, slurry. $^1$H NMR (DMSO-$d_6$, 400 MHz): $\delta$ 3.76 (s, 3H), 3.84 (s, 6H), 7.10 (s, 2H), 7.30 (t, $J$ = 7.8 Hz, 1H), 7.40 (dd, $J$ = 1.1 and 7.4 Hz, 1H), 7.52 (dd, $J$ = 1.3 and 5.0 Hz, 1H), 7.70-7.75 (m, 1H), 7.80-7.86 (m, 1H), 7.93 (s, 1H), 8.23 (dd, $J$ = 1.1 and 7.8 Hz, 1H), 11.86 ppm (br s, disappeared after treatment with $D_2O$, 1H). IR: $v$ 1580 and 2925 cm$^{-1}$. MS (ESI): 394.4 ($MH^+$). $C_{22}H_{19}NO_4S$ (393.46).

*5.1.22. 5-(Thiophen-3-yl)-1H-indole (**30**)*

Synthesized as **16** starting from **23** and 3-thienylboronic acid. Yield 40%, mp 80-83° C (from *n*-hexane), lit. 80-82 °C [43].

*5.1.23. 6-(Furan-2-yl)-1H-indole (**31**).*

Synthesized as **16** starting from **25** and furan-2-boronic acid MIDA ester. Yield 19%, mp 90-96 °C (from *n*-hexane). $^1$H NMR (DMSO-$d_6$, 400 MHz): $\delta$ 6.38-6.42 (m, 1H), 6.50-6.56 (m, 1H), 6.81 (dd, $J$ = 0.8 and 3.4 Hz, 1H), 7.32-7.36 (m, 2H), 7.55 (d, $J$ = 8.3 Hz, 1H), 7.69-7.71 (m, 2H), 11.17 ppm (br s, disappeared after treatment with $D_2O$, 1H). IR: $v$ 3388 cm$^{-1}$.

*5.1.24. 6-(Furan-3-yl)-1H-indole (**32**)*

Synthesized as **16** starting from **25** and furan-3-boronic acid MIDA ester. Yield 7%, mp 155-158 °C (from *n*-hexane). $^1$H NMR (DMSO-$d_6$, 400 MHz): $\delta$ 6.37-6.40 (m, 1H), 6.90-6.95 (m, 1H), 7.25 (dd, $J$ = 1.6 and 8.2 Hz, 1H), 7.30-7.32 (m, 1H), 7.50-7.53 (m, 2H), 7.77 (t, $J$ = 1.8 Hz, 1H), 8.08-8.12 (m, 1H), 11.07 ppm (br s, disappeared after treatment with $D_2O$, 1H). IR: $\nu$ 3384 cm$^{-1}$.

*5.1.25. 7-(Furan-2-yl)-1H-indole (**35**)*

Synthesized as **16** starting from **26** and 2-furanylboronic acid MIDA ester. Yield 21% as an oil [44].

*5.1.26. 7-(Thiophen-2-yl)-1H-indole (**36**)*

Synthesized as **16** starting from **26** and 2-thienylboronic acid. Yield 67% as an oil [45].

*5.1.27. General procedure for the synthesis of derivatives **27** and **29**. Example. 5-(Furan-2-yl)-1H-indole (**27**)*

A mixture of **24** (243 mg, 1 mmol), 2-furanboronic acid (223 mg, 2 mmol), palladium(II) acetate (11 mg, 0.05 mmol), tri(*o*-tolyl)phosphine (30 mg g, 0.1 mmol), potassium phosphate tribasic (745 mg, 3.5 mmol) in ethanol (10 mL) and toluene (5 mL) was heated at 80 °C for 2 h. After cooling, the reaction mixture was diluted with a saturated aqueous solution of sodium hydrogen carbonate and extracted with ethyl acetate. The organic layer was washed with brine, dried and filtered. Evaporation of the solvent gave a residue that was purified by column chromatography (silica gel, *n*-hexane:ethyl acetate = 5:1 as eluent) to give **27** (159 mg, yield 87%), mp 108-110 °C (from ethanol), lit. 110-111 °C.

*5.1.28. 5-(Thiophen-2-yl)-1H-indole (**29**)*

Synthesized as **27** starting from 2-thienylboronic acid. Yield 73%, mp 50-51 °C (from *n*-hexane), lit. 53-54 °C [46].

*5.1.29. Synthesis of 5-(furan-2-yl)-1H-indole (**28**)*

A mixture of **24** (243 mg, 1 mmol), 3-furanboronic acid pinacol ester (253 mg, 1.3 mmol), potassium carbonate (179 mg, 1.3 mmol) in methylpyrrolidone (2 mL) and water (0.15 mL) was degassed for 15 min. Palladium(II) acetate (30 mg, 0.13 mmol) was added, and the reaction mixture was placed into the MW cavity (closed vessel mode, Pmax = 250 psi). Starting MW irradiation of 200 W was used, the temperature being ramped from 25 to 110 °C. Once this was reached, taking around 2 min, the mixture was held at this temperature for 15 min with rapid stirring. The reaction mixture was diluted with water and extracted with ethyl acetate. The organic layer was washed with brine, dried and filtered. Evaporation of the solvent gave a residue that was purified by column chromatography (silica gel, *n*-hexane:ethyl acetate = 5:1 as eluent) to give **28** (82 mg, yield 45%) mp 89-90 °C (from *n*-hexane), lit. 89-91 °C [47].

*5.1.30. Synthesis of 7-iodo-1H-indol-3-yl)(3,4,5-trimethoxyphenyl)methanone (**38**)*

A mixture of **26** (243 mg, 1 mmol), 3,4,5-trimethoxybenzoyl chloride (230 mg, 1 mmol) and anhydrous aluminum chloride (133 mg, 1 mmol) in 1,2-dichloroethane (2 mL) was placed into the MW cavity (closed vessel mode, Pmax = 250 psi). A starting MW irradiation of 150 W was used, the temperature being ramped from 25 to 110 °C with rapid stirring. Once 110 °C was reached, taking around 1 min, the reaction mixture was held at this temperature for 2 min, diluted with water, treated with 1 N HCl and extracted with chloroform. The organic layer was washed with brine, dried and filtered. Evaporation of the solvent gave a residue that was purified by column chromatography (silica gel, *n*-hexane:ethyl acetate = 1:1 as eluent) to give **38** (223 mg, yield 51%, mp 148-153 °C (from ethanol). $^1$H NMR (DMSO-$d_6$, 400 MHz): δ 3.76 (s, 3H), 3.85

(s, 6H), 7.04 (t, *J* = 7,6 Hz, 1H), 7.09 (s, 2H), 7.66 (dd, *J* = 1.0 and 7.6 Hz, 1H), 7,98 (s, 1H), 8.23 (dd, *J* = 1.0 and 7.96 Hz, 1H), 11.86 ppm (br s, disappeared after treatment with $D_2O$, 1H). IR: ν 1577 and 3112 $cm^{-1}$.

*5.2. Molecular Modeling Studies*

All molecular modeling studies were performed on a MacPro dual 2.66GHz Xeon running Ubuntu 14LTS. The tubulin structures were downloaded from the PDB data bank (http://www.rcsb.org/), PDB code: 1SA0 [30], 4O2A [48], 4O2B [48], 5CA0 [8], 5CB4 [8], 5LYJ [49] and 3HKC [50]. Ligand structures were prepared with Maestro [51]. Proteins were prepared by the protein preparation wizard [52] of Maestro. The docking simulations were performed using Plants [53] and Autodock [54]. Images shown in the manuscript were prepared with Pymol [55].

*5.3. Biological assays*

*5.3.1. Tubulin assembly*

The reaction mixtures contained 0.8 M monosodium glutamate (pH 6.6 with HCl in a 2 M stock solution), 10 μM tubulin, 4% (v/v) DMSO, and varying concentrations of drug. Following a 15 min preincubation at 30 °C, samples were chilled on ice, GTP to 0.4 mM was added, and turbidity development was followed at 350 nm in a temperature-controlled recording spectrophotometer for 20 min at 30 °C. The extent of reaction was measured. Full experimental details were previously reported [56].

*5.3.2. [$^3$H]Colchicine binding assay*

The reaction mixtures contained 1.0 μM tubulin, 5.0 μM [$^3$H]colchicine, and 5.0 μM inhibitor and were incubated for 10 min at 37 °C. Complete details were described previously [57].

*5.3.3. Cell cultures*

Cell lines were obtained from the American Type Culture Collection (ATCC), unless otherwise specified. MCF-7 breast carcinoma, OVCAR-8, and NCI/ADR-RES cells were obtained from the National Cancer Institute drug screening laboratory. U87MG and U343MG cell lines were obtained from the National Institute for Cancer Research of Genoa (Italy) and Cell Lines Service GmbH (Germany), respectively. All cell lines, except as indicated, were grown in Dulbecco's modified Eagle's medium (DMEM) supplemented with 10% fetal bovine serum (FBS), 20 mM HEPES, 100 U/mL penicillin, 100 mg/mL streptomycin, and 1% L-glutamine; specific requirements include the addition of glucose (4.5 g/L for HT29 and HCT116 cells; 1 g/L for HepG2). Cell lines were cultured at 37 °C in 5% $CO_2$/95% air in a humidified incubator. Treatments were initiated 24 h after cell seeding using compound **13** or **19** diluted in 0.1% DMSO, the indicated reference compound, or 0.1% DMSO vehicle, for 24-72 h as indicated. T98G and U87MG cells were cultured in RPMI medium and minimum essential medium Eagle, respectively, supplemented with 10% FBS, 2 mM L-glutamine, 100 U/mL penicillin, 100 mg/mL streptomycin and 1% non-essential amino acids at 37 °C in 5% $CO_2$. The U343MG cells were cultured in minimum essential medium Eagle with 2 mM L-glutamine and Earle's BSS adjusted to contain 1.5 mg/mL sodium bicarbonate and supplemented with 10% FBS, 100 U/mL penicillin, 100 mg/mL streptomycin, 1% non-essential amino acids and 1.0 mM sodium pyruvate at 37 °C in 5% $CO_2$.

*5.3.4. Cell viability assays*

The methodology for the evaluation of the growth of human MCF-7 breast carcinoma, OVCAR-8, and NCI/ADR-RES cells, obtained from the National Cancer Institute drug screening laboratory, was previously described, except that cells were grown for 96 h for $IC_{50}$

determinations [58]. Cell viability of HT29, HCT116 and HepG2 cells was determined using the MTT colorimetric assay. HT29, HepG2 and HCT116 cells were seeded into 24-well plates to a density of $15\times10^3$/mL in each well. After 24 h of growth to allow attachment of cells to the wells, test compounds were added at 20-320 nM. After 48 h of growth and removal of the culture medium, 500 µL/well of PBS containing 500 µM MTT was added. Cell cultures were further incubated at 37 °C for 2 h in the dark. The solutions were then gently aspirated from each well, and the formazan crystals within the cells were dissolved in propan-2-ol and 0.04 N HCl (200 µL). Optical densities were read at 550 nm using a Multiskan Spectrum Thermo Electron Corporation reader. The results were expressed as % relative to vehicle-treated control (0.1% DMSO), and $IC_{50}$ values were calculated by nonlinear regression analysis (GraphPad Prism statistics software). The effect of the treatment with compounds **13** or **19** on the T98G, U87MG and U343MG cell lines was estimated using the colorimetric MTS conversion assay, as previously reported.[27] After compound incubations, the MTS reagent was added, and the absorbance at 590 nm was measured by a microplate reader (Wallac, Victor 2, 1420 Multilabel Counter, PerkinElmer). The percentage of proliferating cells after compound exposure was calculated with respect to control cells (100%). The effect of treatment with compounds **13** or **19** on MV4-11, THP-1, A-549 and PC3 cell was determined by CellTiter-Fluor™ (Promega cod. G6082). The cells were seeded in 96 multiwell plates at the indicated densities (MV-4: 5000 cells/50 µL/well; THP-1: 2000 cells/50 µL/well; A549: 3500 cells/50 µL/well; MDA-MB-231: 3500 cells/50 µL/well; PC-3: 2000 cells/50 µL/well). 24 h after plating, compound **13** or **19** was added to the cells, and the effect on cell proliferation was determined after 72 h by the CellTiter-Fluor™ assay. After adding the reagents to the cell plates, the cells were incubated for 90 min at

37 °C, and the fluorescent signal was read by using a TECAN reader. The $IC_{50}$ and $GI_{50}$ results were obtained by analysis with GraphPad Prism and Assay Explorer software.

*5.3.5. Statistical analyses*

Graph-Pad Prism 5 software (Graph-Pad Software Inc, San Diego, CA) was used for data analysis and graphic presentations. Statistical analysis was performed by non-linear regression fitting; sigmoidal-dose response curves were performed using the log(inhibitor) vs response analyses. The $IC_{50}$ value and the maximal efficacy of compounds in inhibiting cell viability (E max) were derived.

*5.3.6. Immunofluorescence and microscopy*

After treatment, HeLa cells directly grown on sterile poly-L-lysine (Sigma P4832) coated coverslips were fixed in methanol for 6 min at -20 °C and processed for IF using mouse α-tubulin antibody (Sigma clone B-5-1-2, 1:3000 dilution) followed by FITC-conjugated anti-mouse secondary antibody (Jackson Immunoresearch Laboratories). Slides were counterstained with 0.05 μg/mL DAPI (Sigma) and mounted in Vectashield (Vector). IF-processed cells were examined under an epifluorescence Nikon Eclipse 90i with a QICAM Fast 1394 (QImaging) camera and using the NIS-Elements AR 4.0 software (Nikon). Single cell images were routinely taken using immersion oil 100x objectives with NA 1.3.

*5.3.7. Flow cytometric analysis*

Cell cycle phase distribution was analyzed after incubation with PI (Sigma P4170). All parameters (FS, SS and FL-3) were acquired in a linear amplification scale. Cell aggregates were gated out on the bi-parametric graph FL-3 lin/ratio. Cell death was analyzed using annexin V-FITC (Immunological Sciences, IK-11120). Cell samples were analyzed in a Coulter Epics XL

cytofluorometer (Beckman Coulter) equipped with EXPO 32 ADC software. Data from at least 10.000 cells per sample were acquired and processed using Win MDI software.

*5.3.8. RNA extraction, reverse transcription and real-time polymerase chain reaction analysis*

Total cellular RNA was processed, and 1 µg of total RNA was retro-transcribed. The cDNA was used to perform a real-time PCR using $p21^{Cip1/Waf1}$ and GAPDH primers as indicated in Table 1S, Supporting Information. For $p21^{Cip1/Waf1}$ and GAPDH genes, the following protocols were used for the PCRs: initialization at 95 ºC for 3 min, followed by 40 cycles of 95 ºC for 10 s, 60 ºC for 10 s, 72 ºC for 10 s. The melting program was 95 ºC for 5 s, 65 ºC for 1 min and 97 ºC for 10 s. The rate of temperature increase was 1 ºC/s, and fluorescence data were continuously acquired. The relative amounts of target genes were normalized to GAPDH expression by Light Cycler® 480 Software version 1.5 (Roche Diagnostics) using the $2\Delta\Delta Ct$ method.

**Acknowledgments**

This research was supported by grants PRIN 2015 n. 2015FCHJ8E (to R.S.), Finanziamenti Ateneo 2016 Sapienza Università di Roma n. RG116154CF287B95 (to G.L.R.), AIRC (Italian Association for Cancer Research, grant n. IG10164 to P.L), and Consiglio Nazionale delle Ricerche Flagship Project InterOmics (to P.L.).

**Disclaimer**

The content of this paper is solely the responsibility of the authors and does not necessarily reflect the official views of the National Institutes of Health.

**Appendix A. Supplementary data**

Supplementary data related to this article can be found at the Journal website.

**References**

[1] E. Nogales. Structural insights into microtubule function. Annual Review of Biochemistry 69 (2000) 277-302.

[2] M.A Jordan, L. Wilson. Microtubules as a target for anticancer drugs. Nature Reviews Cancer 4 (2004) 253-265.

[3] S. Florian, T.J. Mitchison. Anti-microtubule drugs. Methods in Molecula Bioogy 1413 (2016) 403-421.

[4] I. Marzo, J. Naval. Antimitotic drugs in cancer chemotherapy: promises and pitfalls. Biochemical Pharmacology 86 (2013) 703-710.

[5] E. Mukhtar, V.M. Adhami, H. Mukhtar. Targeting microtubules by natural agents for cancer therapy. Molecular Cancer Therapeutics 13 (2014) 275-284.

[6] G. Chandrasekaran, P. Tatrai, F. Gergely. Hitting the brakes: targeting microtubule motors in cancer. British Journal of Cancer 113 (2015) 693-698.

[7] B. Bhattacharyya, D. Panda, S. Gupta, S. Banerjee, M. Anti-mitotic activity of colchicine and the structural basis for its interaction with tubulin. Medicinal Research Review 28 (2008) 155-183.

[8] R.B. Ravelli, B. Gigant, P.A. Curmi, I. Jourdain, S. Lachkar, A. Sobel, M. Knossow, Insight into tubulin regulation from a complex with colchicine and a stathmin-like domain. Nature 428 (2004) 198-202.

[9] C.M. Lin, H.H. Ho, G.R. Pettit, E. Hamel. Antimitotic natural products combretastatin A-4 and combretastatin A-2: studies on the mechanism of their inhibition of the binding of colchicine to tubulin. Biochemistry 28 (1989) 6984-6991.

[10] T. Beckers, S. Mahboobi. Natural, semisynthetic and synthetic microtubule inhibitors for

cancer therapy. Drugs of the Future 28 (2003) 767-785.

[11] E. Nogales, M. Whittaker, R.A. Milligan, K.H. Downing. High-resolution model of the microtubule. Cell 96 (1999) 79-88.

[12] J.H. Nettles, H. Li, B. Cornett, J.M. Krahn, J.P. Snyder, K.H. Downing. The binding mode of epothilone A on alpha, beta-tubulin by electron crystallography. Science 2004, 305, 866-869.

[13] R.M. Buey, E. Calvo, I. Barasoain, O. Pineda, M.C. Edler, R. Matesanz, G. Cerezo, C.D. Vanderwal, B.W. Day, E.J. Sorensen, J.A. Lopez, J.M. Andreu, E. Hamel, J.F. Diaz. Cyclostreptin binds covalently to microtubule pores and lumenal taxoid binding sites. Nature Chemical Biology 3 (2007) 117-125.

[14] Y.M. Liu, H.L. Chen, H.Y. Lee, J.P. Liou. Tubulin inhibitors: a patent review. Expert Opinion on Therapeutic Patents 24 (2014) 69-88.

[15] J.J. Field, A. Kanakkanthara, J.H. Miller Microtubule-targeting agents are clinically successful due to both mitotic and interphase impairment of microtubule function. Bioorganic and Medicinal Chemistry 22 (2014) 5050-5059.

[16] X. Wu, Q. Wang, W. Li. Recent advances in heterocyclic tubulin inhibitors targeting the colchicine binding site. Anti-cancer Agents in Medicinal Chemistry 16 (2016) 1325-1338.

[17] D. Cella, A. Peterman, S. Hudgens, K. Webster, M.A. Socinski, M.A. Measuring the side effects of taxane therapy in oncology: the functional assesment of cancer therapy-taxane (FACT-taxane). Cancer 98 (2003) 822-831.

[18] B. Kumar, R. Kumar, I.I. Skvortsova, V Kumar. Mechanisms of tubulin binding ligands to target cancer cells: updates on their therapeutic potential and clinical trials. Current Cancer Drug Targets 17 (2017) 357-375.

[19] D. Fanale, G Bronte, F. Passiglia, V. Calò, M. Castiglia, F. Di Piazza, N. Barraco, A. Cangemi, M.T. Catarella, L. Insalaco, A. Listì, R. Maragliano, D. Massihnia, A. Perez, F. Toia, G. Cicero, V. Bazan. Stabilizing versus destabilizing the microtubules: a double-edge sword for an effective cancer treatment option? Analytical Cellular Pathology (Amsterdam) 2015 (2015) 690-916.

[20] Y. Lu, J.J. Chen, M. Xiao, W. Li, D.D. Miller. An overview of tubulin inhibitors that interact with the colchicine binding site. Pharmaceutical Research 29 (2012) 2943-2971.

[21] C. Kanthou, G.M. Tozer. Microtubule depolymerizing vascular disrupting agents: Novel therapeutic agents for oncology and other pathologies. International Journal of Experimental Pathology 90 (2009) 284-294.

[22] C. Stengel, S.P. Newman, M.P. Leese, B.V. Potter, M.J. Reed, A. Purohit. Class III beta-tubulin expression and in vitro resistance to microtubule targeting agents. British Journal of Cancer 102 (2010) 316-324.

[23] D. Carta, M.G. Ferlin. An overview on 2-arylquinolin-4(1*H*)-ones and related structures as tubulin polymerisation inhibitors. Current Topics in Medicinal Chemistry 14, (2014) 2322-2345.

[24] R. Patil, S.A. Patil, K.D. Beaman, S.A. Patil. Indole molecules as inhibitors of tubulin polymerization: potential new anticancer agents, an update (2013-2015). Future Medicinal Chemistry 8 (2016) 1291-1316.

[25] G. La Regina, R. Bai, W.M. Rensen, E. Di Cesare, A. Coluccia, F. Piscitelli, V. Famiglini, A. Reggio, M. Nalli, S. Pelliccia, E. Da Pozzo, B. Costa, I. Granata, A. Porta, B. Maresca, A. Soriani, M.L. Iannitto, A. Santoni, J. Li, M.M. Cona, F. Chen, Y. Ni, A. Brancale, G. Dondio, S. Vultaggio, M. Varasi, C. Mercurio, C. Martini, E. Hamel, P.

Lavia, E. Novellino, R. Silvestri. Towards highly potent cancer agents by modulating the C-2 group of the arylthioindole class of tubulin polymerization inhibitors. Journal of Medicinal Chemistry 56 (2013) 123-149.

[26] G. La Regina, R. Bai, W.M. Rensen, A. Coluccia, F. Piscitelli, V. Gatti, A. Bolognesi, A. Lavecchia, I. Granata, A. Porta, B. Maresca, A. Soriani, M.L. Iannitto, M. Mariani, A. Santoni, A. Brancale, C. Ferlini, G. Dondio, M. Varasi, C. Mercurio, E. Hamel, P. Lavia, E. Novellino, R Silvestri. Design and synthesis of 2-heterocyclyl-3-arylthio-1*H*-indoles as potent tubulin polymerization and cell growth inhibitors with improved metabolic stability. Journal of Medicinal Chemistry 54 (2011) 8394-8406.

[27] G. La Regina, R. Bai, A. Coluccia, V. Famiglini, S. Pelliccia, S. Passacantilli, C. Mazzoccoli, V. Ruggieri, A. Verrico, A. Miele, L. Monti, M. Nalli, R. Alfonsi, L. Di Marcotullio, A. Gulino, B. Ricci, A. Soriani, A. Santoni, M. Caraglia, S. Porto, E. Da Pozzo, C. Martini, A. Brancale, L. Marinelli, E. Novellino, S. Vultaggio, M. Varasi, C. Mercurio, C. Bigogno, G. Dondio, E. Hamel, P. Lavia, R. Silvestri. New indole tubulin assembly inhibitors cause stable arrest of mitotic progression, enhanced stimulation of natural killer cell cytotoxic activity, and repression of Hedgehog-dependent cancer. Journal of Medicinal Chemistry 58 (2015) 5789-5807.

[28] G. La Regina, V. Gatti, V. Famiglini, F. Piscitelli, R. Silvestri. Venting-while-heating microwave-assisted synthesis of 3-arylthioindoles. ACS Combinatorial Science 14 (2012) 258-262.

[29] G. De Martino, G. La Regina, A Coluccia, M.C. Edler, M.C. Barbera, A. Brancale, E. Wilcox, E. Hamel, M. Artico, R. Silvestri. Arylthioindoles, potent Inhibitors of tubulin polymerization. Journal of Medicinal Chemistry 47 (2004) 6120-6123.

[30] A. Coluccia, D. Sabbadin, A. Brancale. Molecular modelling studies on arylthioindoles as potent inhibitors of tubulin polymerization. European Journal of Medicinal Chemistry 46 (2011) 3519-3525.

[31] Y. Wang, H. Zhang, B. Gigant, Y. Yu, Y. Wu, X. Chen, Q. Lai, Z. Yang, Q. Chen, J. Yang. Structures of a diverse set of colchicine binding site inhibitors in complex with tubulin provide a rationale for drug discovery. The FEBS Journal 283 (2016) 102-111.

[32] T. Simonart, G. Andrei, D. Parent, J.P. Van Vooren, E. De Clercq, R. Snoeck. In vitro sensitivity of Kaposi's sarcoma cells to various chemotherapeutic agents including acyclic nucleoside phosphonates. Antiviral Chemistry and Chemotherapy 10 (1999) 129-134.

[33] H.H. Ryu, S. Jung, T.Y. Jung, K.S. Moon, I.Y. Kim, Y.L. Jeong, S.G. Jin, J. Pei, M. Wen, W.Y. Jang. Role of metallothionein 1E in the migration and invasion of human glioma cell lines. International Journal of Oncology 41 (2012) 1305-1313.

[34] C.A. Lipinski, F. Lombardo, B.W. Dominy, P.J. Feeney. Experimental and computational approaches to estimate solubility and permeability in drug discovery and development settings. Advanced Drug Delivery Reviews 46 (1997) 3–26.

[35] D.F. Veber, S.R. Johnson, H.Y. Cheng, B.R. Smith, K.W. Ward, K.D. Kopple. Molecular properties that influence the oral bioavailability of drug candidates. Journal of Medicinal Chemistry 45 (2002) 2615-2623.

[36] D. Lagorce, O. Sperandio, J.B. Baell, M.A. Miteva, B.O.Villoutreix. FAF-Drugs3: a web server for compound property calculation and chemical library design. Nucleic Acids Research 43 (Web Server issue) (2015) W200-W207.

[37] J.D. Hughes, J. Blagg, D.A. Price, S. Bailey, G.A. Decrescenzo, R.V. Devraj, E. Ellsworth, Y.M. Fobian, M.E. Gibbs, R.W. Gilles, N. Greene, E. Huang, T. Krieger-

Burke, J. Loesel, T. Wager, L. Whiteley, Y. Zhang. Physiochemical drug properties associated with *in vivo* toxicological outcomes. Bioorganic and Medicinal Chemistry Letters 18 (2008) 4872-4875.

[38] T. Cheng, Y. Zhao, X. Li, F. Lin, Y. Xu, X. Zhang, Y. Li, R. Wang, L. Lai. Computation of octanol-water partition coefficients by guiding an additive model with knowledge. Journa of Chemical Information and Modeling 47 (2007) 2140-2148.

[39] J.S. Delaney. ESOL: estimating aqueous solubility directly from molecular structure. Journal of Chemical Information and Computer Sciences 44 (2004) 1000-1005.

[40] H. Pajouhesh, G.R. Lenz. medicinal chemical properties of successful central nervous system drugs. NeuroRx. 2 (2005) 541–553.

[41] S.K. Carlsson, S.P. Brothers, C. Wahlestedt. Emerging treatment strategies for glioblastoma multiforme. EMBO Molecular Medicine 6 (2014) 1359-1370.

[42] J. Cmielová, M. Rezáčová. p21Cip1/Waf1 protein and its function based on a subcellular localization. Journal of Cellular Biochemistry 112 (2011) 3502-3506.

[43] K. Billingsley, S.L. Buchwald. Highly efficient monophosphine-based catalyst for the palladium-catalyzed Suzuki-Miyaura reaction of heteroaryl halides and heteroaryl boronic acids and esters. Journal of the American Chemical Society 129 (2007) 3358-3366.

[44] M.L. Read, A. Krapp, P.O. Miranda, L.-L. Gundersen. Synthesis of complex fused polycyclic heterocycles utilizing IMDAF reactions of allylamino- or allyloxy-furyl(hetero)arenes. Tetrahedron 68 (2012) 1869-1885.

[45] L. Wiesemann, M. Kleih, H.A. Mayer. Aromatic aza-bicyclic compounds comprising Cu, Ag, Au, Zn, Al for use in electroluminescent devices. PCT Int. Appl. WO 2014067598 A1, September 13, 2013.

[46] T. Tsuchimoto, Y. Iketani, M. Sekine. Zinc-catalyzed dehydrogenative *N*-silylation of indoles with hydrosilanes. Chemistry – A European Journal 18 (2012) 9500-9504.

[47] M.A. Oberli, S.L. Buchwald. A general method for Suzuki-Miyaura coupling reactions using lithium triisopropyl borates. Organic Letters 14 (2012) 4606-4609.

[48] A.E. Prota, F. Danel, F. Bachmann, K. Bargsten, R.M. Buey, J. Pohlmann, S. Reinelt, H. Lane, M.O. Steinmetz. The novel microtubule-destabilizing drug BAL27862 binds to the colchicine site of tubulin with distinct effects on microtubule organization. Journal of Molecular Biology 426 (2014) 1848-1860.

[49] R. Gaspari, A.E. Prota, K. Bargsten, A. Cavalli, M.O. Steinmetz. Structural basis of cis- and trans-combretastatin binding to tubulin. Chem 2 (2017) 102-113.

[50] A. Dorleans, B. Gigant, R.B.G. Ravelli, P. Mailliet, V. Mikol, M. Knossow. Variations in the colchicine-binding domain provide insight into the structural switch of tubulin. Proceedings of the National Academy of Sciences of the United States of America 106 (2009) 13775-13779.

[51] Schrödinger Release 2017-3: Maestro, Schrödinger, LLC, New York, NY, 2017.

[52] G.M. Sastry, M. Adzhigirey, T. Day, R. Annabhimoju, W. Sherman. Protein and ligand preparation: Parameters, protocols, and influence on virtual screening enrichments. Journal of Computer-Aided Molecular Design 27 (2013) 221-234.

[53] O. Korb, T. Stutzle, T.R. Exner. Plants: application of ant colony optimization to structure-based drug design. In Ant Colony Optimization and Swarm Intelligence, Proceedings of the 5$^{th}$ International Workshop, Ants; M. Dorigo, L.M. Gambardella, M. Birattari, A. Martinoli, R. Poli, T. Stutzle, Eds. Lecture Notes in Computer Science, Series 4150, Springer, Berlin 2006, pp 247-258.

[54] G. M. Morris, R. Huey, W. Lindstrom, M.F. Sanner, R.K. Belew, D.S. Goodsell, A.J. Olson. Autodock4 and AutoDockTools4: automated docking with selective receptor flexiblity. Journal of Computational Chemistry 16 (2009) 2785-2791.

[55] The Pymol Molecular Graphics System, Version 2.0 Schrödinger, LLC.

[56] E. Hamel, E. Evaluation of antimitotic agents by quantitative comparisons of their effects on the polymerization of purified tubulin. Cell Biochemistry and Biophysics 38 (2003) 1-21.

[57] P. Verdier-Pinard, J.-Y Lai, H.-D. Yoo, J. Yu, B. Marquez, D.G. Nagle, M. Nambu, J.D. White, J.R. Falck, W.H. Gerwick, B.W. Day, E. Hamel. Structure-activity analysis of the interaction of curacin A, the potent colchicine site antimitotic agent, with tubulin and effects of analogs on the growth of MCF-7 breast cancer cells. Molecular Pharmacology 35 (1998) 62-76.

[58] S. Ruan, M.F. Okcu, R.C. Pong, M. Andreeff, V. Levin, J.T. Hsieh, W. Zhang, W. Attenuation of WAF1/Cip1 expression by an antisense adenovirus expression vector sensitizes glioblastoma cells to apoptosis induced by chemotherapeutic agents 1,3-bis(2-chloroethyl)-1-nitrosourea and cisplatin. Clinical Cancer Research 5 (1999) 197-202.

*Manuscript title:* New 6- and 7-heterocyclyl-1*H*-indole derivatives as potent tubulin assembly and cancer cell growth inhibitors

*Research Highlights*

- 3-Arylthio- and 3-aroyl-1*H*-indoles bearing a heterocyclic ring were synthesized.
- The 6- and 7-heterocyclyl-1*H*-indoles are potent anticancer agents.
- Compounds **13** and **19** inhibit MDR cell line at low nanomolar concentrations.
- Compound **13** is a potent inhibitor of the human U87MG glioblastoma cells.
- Compound **13** causes 50% stable arrest of mitosis in HeLa cells.